Advanced Virgo Technical Design Report

VIR–xxxA–12

Issue 2

The Virgo Collaboration

February 8, 2012

Contents

Chapter 1

ISC

1.1 General description of the sub-system

The Interferometer Sensing and Control (ISC) subsystem of the Advanced Virgo project deals with the design of the control systems that will be used both during the lock acquisition of the interferometer and the steady state (Science Mode) operations.

The design requirement to the ISC subsystem are:

- Develop a control strategy capable of maintaining the interferometer controlled at the design sensitivity with good stability and duty cycle. This means that all control loops must have large enough stability margins and that all control noises re-introduced by the loops must contribute at maximum a factor 10 below the design sensitivity.
- Develop a repeatable and robust lock acquisition strategy, capable of bringing the interferometer from a fully uncontrolled state to the final, good sensitivity one in a reasonably short time (of the order of tens of minutes).
- All of the above must be obtained for at least three different optical configurations: power-recycled only interferometer at low input power (chosen to be 25 W as reference); dual-recycled interferometer at low input power; dual-recycled interferometer at full input power (125 W).

The degrees of freedom to be controlled are divided in longitudinal and angular ones (refer to sec. 1.3.1 and 1.7.2 for definitions). Since the cross-coupling between the two sets is typically not dominant, the control system design can be carried out separately. In the longitudinal case it is necessary to distinguish between the lock acquisition state and the steady state. In the angular control system case there is no need for such a distinction, since

global control loops will be activated only when the interferometer is already close enough to the final working point.

All the designs described in the following sections have been obtained using simulations of the full interferometer based on modal models. The two main frequency-domain tools used so far are Finesse [1] and Optickle [2]. Both tools are to some extent incomplete: Finesse can introduce higher order modes but cannot deal with radiation pressure effects; on the other hand Optickle can deal with radiation pressure but is limited to only the first higher order mode. These limitations are particularly relevant in the design of the angular control system.

Time-domain simulations were also used for the study of the lock acquisition procedures. The choice was to use the e2e [3] software, developed by the LIGO Scientific Collaboration, since it is well maintained and widely used for the design of Advanced LIGO lock acquisition.

Optical simulations of thermal effects and mirror defects inside the power recycling cavity (PRC) showed a large impact on radio-frequency sideband aberrations. A risk reduction strategy to have error signals less sensitive to PRC defects and aberrations is proposed. It will help in the first commissioning and locking steps (sec. 1.6).

1.2 Input from other sub-systems and basic assumptions

All the main beams exiting from the interferometer (reflection, power recycling pick-off, dark port, transmission of the two arms) need to be probed with suitable photo-diodes and quadrant photo-diodes for control and monitoring purposes. A scheme of the interferometer layout with the naming convention is shown in fig. 1.1.

The DET sub-system fixed the amount of power that can be sensed by each longitudinal photo-diode to 50 mW. They plan to install two photo-diodes per port under vacuum, to used in science mode. Therefore the longitudinal control design has been carried out considering that a total of 100 mW is sensed with the longitudinal photo-diodes. The total sensing noise is required to be dominated by the corresponding shot noise. In other words electronic noise in the photo-diode electronic is considered to be negligible with respect to the shot noise [37, 38]. See sec. 1.3.6 for more details.

Similarly DET fixed the amount of power that can be sensed on each quadrant photo-diode to 25 mW for each port [5], except for the dark port before the output mode cleaner (OMC) where the power per quadrant is reduced

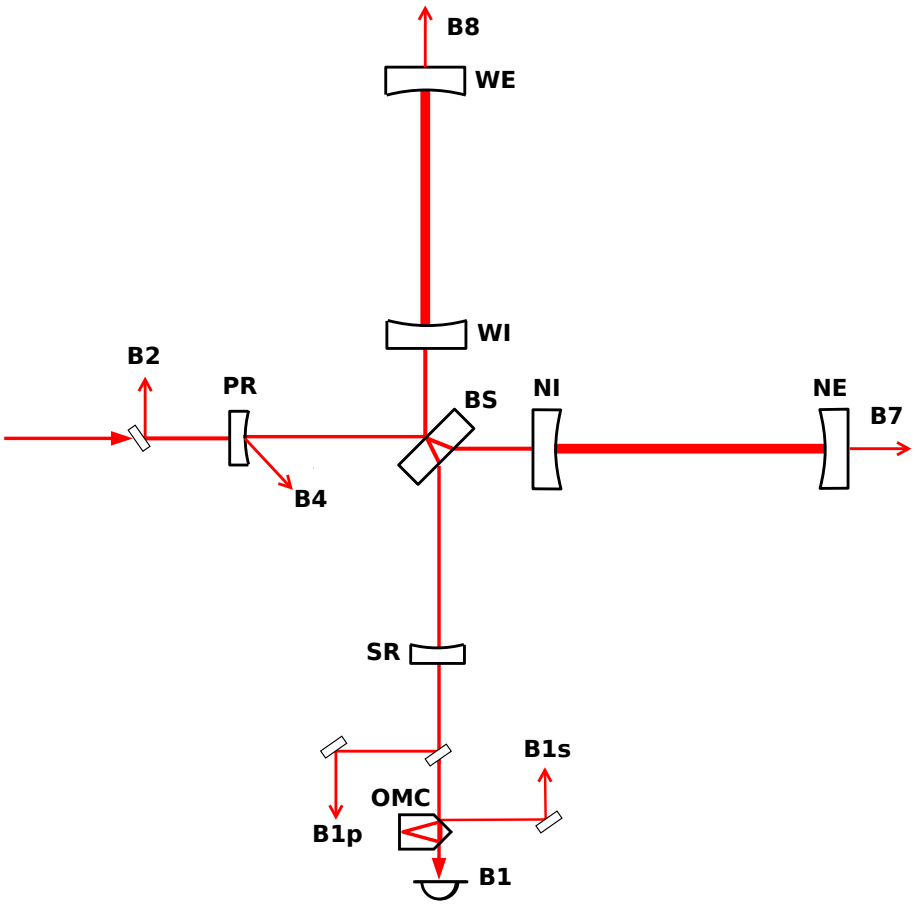

Figure 1.1: Optical layout of the Advanced Virgo interferometer, with mirrors and output ports naming convention.

to 2.5 mW to avoid losing too much of the main beam. In the control design the corresponding sensing noise is again required to be dominated by the corresponding shot noise (sec. 1.7.6), thus considering other sources of noise (electronic and bench motion) to be negligible with respect to it.

The gravitation channel extraction foresee the use of a DC read-out technique. It implies the addition of an offset on one of the differential degrees of freedom to add a local oscillator carrier field at the dark port. The amount of carrier power at the dark port was fixed by DET to be 80 mW [40], based on considerations explained for example in [39].

A frontal modulation technique will be used to control all longitudinal degrees of freedom, except the DARM one, and most of the angular degrees of freedom. Three modulation frequencies are foreseen in steady state conditions. Their values must be chosen, together with the optical path lengths

inside the interferometer, in order to meet the following requirements:

- all modulation frequencies must be transmitted by the input mode cleaner (IMC);
- the first two modulation frequencies must be resonant inside the PRC;
- the third modulation frequency must be anti-resonant inside the PRC;
- the second modulation frequency must be resonant also inside the signal recycling cavity (SRC);
- the transmission of the first modulation frequency to the dark port must be as small as possible.

All these requirements constrain the possible frequencies and distances between mirrors. Considering also the requirements coming from infrastructure and vacuum the set of lengths and modulation listed in the OSD chapter are obtained (sec. [OSD chapter] and tab. 1.1).

The present design of the INJ sub-system foresee the ability of delivering a modulation index of 0.1 for all main modulation frequencies.

The longitudinal and angular control system have been designed starting from the assumption that the mirror residual motions at low frequency will be of the same order of magnitude of those obtained in Virgo: about 0.5 μm and 0.1 μrad RMS concentrated below few Hz.

The Advanced Virgo detector in dual recycled configuration is expected to work with different tunings of the SRC. In the design of both angular and longitudinal control systems only the one which optimizes the sensitivity for NS-NS inspirals has been considered. The SRC tuning will be controlled changing the offset added to the signal recycling cavity length (SRCL) error signal. The available linear range is about double of the tuning corresponding to the NS-NS-optimized configurations. The effect of using different tunings on the control loops and on noise couplings has not been studied yet.

1.3 Longitudinal control system: steady state control

The optical response of the interferometer to longitudinal motions of the mirrors has been simulated using Optickle [2] which is as of today the only tool capable of including radiation pressure effects. Three different configurations have been considered for all the design steps: power-recycled only

Parameter	Value
Power recycling mirror transmission	0.05
Input mirror transmission	0.014
End mirror transmission	1 ppm
Signal recycling mirror transmission	0.2
Losses per mirror	32.5 ppm
Arm cavity mirror mass	42 kg
Power recycling cavity length	11.952 m
Signal recycling cavity length	11.952 m
Schnupp asymmetry	0.23 m
Arm cavity length	2999.8 m
Modulation frequencies	$f_1 = 6270777$ Hz
	$f_2 = 56436993$ Hz
	$f_3 = 8361012$ Hz
Suspension last stage resonant frequency	600 mHz
DC readout offset	see tab. 1.3
Signal recycling cavity detuning	3.022×10^{-7} m

Table 1.1: List of relevant parameters used in the Optickle simulation. Reference from [8].

interferometer at low input power, namely 25 W; dual recycled interferometer at low input power (25 W); dual recycled interferometer at full input power, namely 125 W.

The main parameters used in the simulation are summarized in tab. 1.1. More details on the longitudinal control can be found in the note [6].

1.3.1 Definition of degrees of freedom

In a dual recycled interferometer the length sensing and control system deals with five degrees of freedom. Referring to fig. 1.2, the microscopic positions (*tunings*) of all mirrors are combined to obtain the following physical degrees of freedom:

$$\begin{aligned} DARM &= \frac{L_N - L_W}{2} \\ CARM &= \frac{L_N + L_W}{2} \\ MICH &= l_N - l_W \\ PRCL &= l_P + \frac{l_N + l_W}{2} \\ SRCL &= l_S + \frac{l_N + l_W}{2} \end{aligned}$$

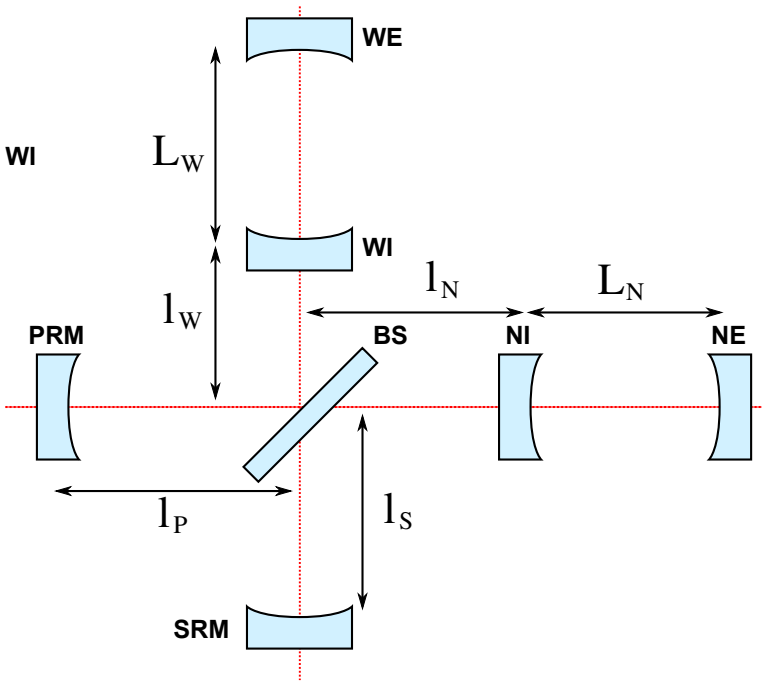

Figure 1.2: Scheme of relevant physical distances between mirrors in a dual recycled interferometer.

The simplest extension of Virgo driving to Advanced Virgo consists in controlling MICH / PRCL / SRCL using PR / SR / BS. Table 1.2 summarizes the driving matrix for a dual recycled interferometer as it is used in all the following simulations.

In addition to these "mechanical" degrees of freedom one should consider the laser frequency stabilization loop, which locks the laser to the mean length of the two arm cavities with typical band-widths of few tens of kHz (sec. 1.3.9). The laser frequency will follow the motion of the arm cavity mean length, called CARM in the previous equations. The typical motion of the CARM degree of freedom, if left free, would correspond to thousands of Hz. To

Mirror/DOF	DARM	CARM	MICH	PRCL	SRCL
NE	$-1/2$	-1			
WE	$1/2$	-1			
BS			$1/\sqrt{2}$		
PR			$-1/2$	-1	
SR			$1/2$		-1

Table 1.2: Driving coefficients for dual recycled interferometer. In the case of power recycled only interferometer the SR driving is simply removed.

avoid such large fluctuation the CARM mechanical mode will be controlled, acting on the end mirrors, using an error signal coming from the reference cavity [18]. This is the same strategy adopted in Virgo+ and allowed also to extract complete position information to be used for the Global Inverted Pendulum Control (GIPC) system.

1.3.2 Definition of available output ports and signals

There are many output ports foreseen in Advanced Virgo:

- The dark fringe or asymmetric port: before the OMC a small fraction is extracted and sent to B1p. The transmission of the OMC is B1 and the reflection is B1s. Since the OMC should filter all sidebands, B1 contains only the fundamental mode carrier field, while all higher order modes and sidebands should therefore go in B1s. For steady state longitudinal control only B1 is used.

- The interferometer reflection or symmetric port, named B2. The amount of power available in this port depends largely on the impedance matching between the PR mirror and the arm cavities reflectivities, which is in turn determined by their round trip losses.

- The transmission of the two arm cavities, named B7 and B8 for north and west respectively. They will not be used for the longitudinal steady state control.

- The power recycling cavity pick-off port (B4), which will be extracted using a plate in front of the power recycling mirror.

The beam is frontal modulated at three radio frequencies listed in tab. 1.1, using electro-optical modulators placed before the input mode cleaner, with modulation indexes set to 0.1. The frequencies must therefore be multiples of the IMC free spectral range. Not all the possible demodulated signals will be needed at all ports: the B1 beam will not see any sideband, so demodulation is useless on that port; f_3 is anti-resonant in the recycling cavity, so signals demodulated at this frequency will be useful only in the B2 beam; the B4 beam finally will contain both f_1 and f_2 sidebands and will provide useful signals at both demodulations. The name convention for signals is: PORT_SBx_yy where x refer to the modulation frequency and can range from 1 to 3, while yy can be DC, P or Q referring respectively to power signal, demodulated in-phase and demodulated quadrature channels. Demodulation phase is chosen in each configuration in order to maximize one chosen degree of freedom in P over Q. Details are given for each configuration separately.

The total power which is sensed at each longitudinal photo-diode is 100 mW, according to specifications given by the DET subsystem [5]. All signals are considered limited by the corresponding shot noise, meaning that all sources of electronic noise are required to be negligible.

The reflectivity of the power recycling pick-off plate (POP) was chosen to be 300 ppm. This will provide 100 mW for the longitudinal photo-diodes and 50 mW for the quadrant diodes for input power larger than 14 W. In this way it will be possible to fully exploit the shot-noise limited sensitivity since the first commissioning steps.

1.3.3 DC readout offset

The DC-readout scheme foresees the addition of an offset to a differential degree of freedom, in order to have a static carrier field reaching the dark port, to be used as phase reference for homodyne detection. In principle it is possible to generate such a static field both with an offset in DARM or MICH. The use of a DARM offset introduces a detuning of the arm cavities from resonance, thus in principle increasing the influence of radiation pressure. Instead using a MICH offset does not move the arm cavities out of resonance. In the presence of a SRC the distinction is however not straightforward. One important point is how optical transfer functions change with the offset, in particular the DARM one and the power and frequency noise couplings.

Results detailed in [6] show that the behavior is different in power recycled and dual recycled configuration. In power recycled only case, if the offset is added to MICH instead of DARM, there is no more any effect of radiation pressure in the DARM optical transfer function. Moreover, in the case of MICH offset, the coupling of frequency and power noises to the output signal is lower, at least in the more critical low frequency region. Therefore the use of a MICH offset is preferable in the case of power recycled only interferometer.

The situation is different in the dual recycled case. Since the DARM optical transfer function is dominated by radiation pressure effects due to the SRC, there is no difference wherever the offset is added. Frequency and power noises instead couple more if a MICH offset is used. It is then preferable to use a DARM offset in the dual recycled case.

In conclusion, in the following simulations, a MICH offset is used in the power recycled interferometer and a DARM one in the dual recycled case. In all three configuration the offset is tuned in order to have 80 mW of carrier fundamental mode power at the dark port. The resulting offsets are summarized in table 1.3.

Configuration	degree of freedom (DOF)	Offset [m]
Power recycled 25W	MICH	$1.6 \cdot 10^{-9}$
Dual recycled 25W	DARM	$2.3 \cdot 10^{-11}$
Dual recycled 125W	DARM	$1.0 \cdot 10^{-11}$

Table 1.3: Offsets needed for reaching 80 mW of power at dark port.

DOF	Power rec. 25W	Dual rec. 25W	Dual rec. 125W
DARM	$6 \cdot 10^{-16}$ m	$2 \cdot 10^{-15}$ m	$1 \cdot 10^{-15}$ m
Frequency		7 mHz	
CARM		$4 \cdot 10^{-13}$ m	
MICH	$2 \cdot 10^{-13}$ m	$6 \cdot 10^{-13}$ m	$3 \cdot 10^{-13}$ m
PRCL		2×10^{-11} m	
SRCL			$3 \cdot 10^{-13}$ m

Table 1.4: Summary of accuracy requirements for longitudinal control loops.

Moreover, the value of the differential offset (on MICH or DARM) has a strong influence on the angular sensing matrix: the larger the offset, the less diagonal the sensing matrix. Therefore the value of the offset should be maintained as small as possible to improve the angular control system robustness [9].

1.3.4 Accuracy requirements

The accuracy requirements for longitudinal loops are summarized in tab. 1.4. The reasoning used to derive these numbers is explained in the note [6]. Here only the considerations for DARM and CARM are repeated, since these accuracy requirements are those having stronger impacts on interfaces with other sub-systems.

In the DARM case the most stringent requirement comes from the use of DC readout. Indeed the response of the dark fringe power to differential motion is intrinsically non-linear: the DC power at B1 varies with very good approximation as a parabola centered at zero offset. The optical gain is given by the derivative of this parabola and therefore it varies linearly even around the nominal operating point.

In general the power at dark port can be described by the following equation:

$$B1 = b_0 + \alpha\delta z + \beta\delta z^2 \tag{1.1}$$

where δz is the residual motion of DARM. The coefficients α and β can be obtained from simulations. However their dependence on the DC read-out offset is easily computed, considering the quadratic nature of the B1 power

response to DARM motion: β is constant and $\alpha = 2z_0\beta$ where z_0 is the static offset.

One of the effects of the non-linear term in the above equation is to create up-conversion of low frequency residual DARM motion around high frequency lines. Indeed, the previous equation is correct in the time domain:

$$b(t) = b_0 + \alpha\delta z(t) + \beta\delta z(t)^2 \tag{1.2}$$

which in frequency domain becomes:

$$\tilde{b}(f) = \alpha\tilde{\delta z}(f) + \beta(\tilde{\delta z} \star \tilde{\delta z})(f) \tag{1.3}$$

If we assume the DARM motion to be composed of a low frequency part (residual motion) and of a large spectral line (like for example violin modes) the convolution can be easily computed and the signal on the diode at the line frequency will be

$$\tilde{b}(f) = \alpha z_L \left(1 + \frac{2\beta}{\alpha} z_{RMS}\right) \delta(f - f_L) \tag{1.4}$$

where z_L and f_L are the amplitude and frequency of the line and z_{RMS} is the residual DARM motion. The second term inside the brackets gives the level of low frequency up-converted noise which falls around the main line. This noise couples directly to the detector sensitivity, thus it must be required to be a factor 10 below the design sensitivity. Assuming to have lines with a signal to noise ratio (SNR) of 1000, which is typical of violin and mirror modes, the term must satisfy:

$$\frac{2\beta}{\alpha} z_{RMS} < \frac{1}{10} \cdot \frac{1}{1000} = 10^{-4} \tag{1.5}$$

From the relation between α and β one finally find the following relation which gives the requirement for DARM:

$$\frac{z_{RMS}}{z_0} < 10^{-4} \tag{1.6}$$

which means that the DARM accuracy must be a factor 10^4 smaller than the actual static offset. This means that for power recycled only configuration at 25 W DARM accuracy must be at the level of $6 \cdot 10^{-16}$ m; for dual recycled at 25 W at $2 \cdot 10^{-15}$ m; for dual recycled at 125 W at $1 \cdot 10^{-15}$ m.

In the CARM case, the very low frequency absolute fluctuation of the laser frequency is dominated by the residual motion of the arm cavity mean length. This is at first order not relevant for the interferometer except for the presence of the output mode cleaner. Indeed any fluctuation of the laser frequency will be equivalent to a change in the length of the OMC and will

at some level spoil its lock accuracy. If an accuracy δz_{OMC} is needed for avoid the re-introduction of OMC length noise in the sensitivity [10], the corresponding tolerable residual motion of the mean arm length is given by

$$\delta z_{CARM} \sim \frac{L_{ARM}}{L_{OMC}} \cdot \delta z_{OMC} \tag{1.7}$$

Assuming for example a length of the OMC of about 30 cm [11] and a level of length noise of the OMC of the order of $4 \cdot 10^{-17}$ m/$\sqrt{\text{Hz}}$ at 10 Hz, the required accuracy for OMC lock is of the order of $4 \cdot 10^{-13}$ m. This corresponds to a CARM lock accuracy of $4 \cdot 10^{-9}$ m or 400 Hz in term of laser frequency. In the baseline design, the CARM slow loop will use, as in Virgo+, an error signal in reflection of the reference cavity, with typical bandwidths of few Hz. Alternative schemes are being considered [11], such as controlling the CARM loop directly using the OMC error signal.

1.3.5 Consequences of the accuracy requirements on OMC filtering

In an ideal world only the carrier fundamental mode is transmitted by the OMC. However in reality, parts of the sidebands and of higher order modes also leaks through the OMC. If these leakage fields fluctuate in amplitude, they will give rise to spurious power fluctuations of the dark fringe photo-diode which will be interpreted by the DARM loop as a motion of the physical degree of freedom.

The maximum leakage power which is tolerable depends on the required DARM accuracy and on the expected power fluctuation of the leaking field. The latter is quite difficult to predict. However a reasonable estimate can be obtained looking at the residual intensity fluctuation of sideband fields at the dark port during the last Virgo+ science run. It turned out that sideband power fluctuates typically of about 2%, coherently with interferometer motions especially in the micro-seismic region [11].

Since at low frequency (below about 1 Hz) the DARM loop has very high gain, any spurious power fluctuation at the dark port is directly converted into a real motion of the DARM degree of freedom, with a conversion factor given by the *purely optical* transfer function of the interferometer. This spurious motion of DARM induced by the loop is not measurable in any way, since the error signal will be squeezed to zero by the high loop gain.

The word purely optical in the last paragraph is relevant in a radiation pressure dominated regime. Radiation pressure creates an opto-mechanical modification of the transfer function. Any force applied to the DARM degree of freedom creates a potential displacement of the same degree of freedom.

Configuration	Optical gain (G)	Requirements
Power recycled 25W	$2.8 \cdot 10^{10} W/m$	0.08 mW
Dual recycled 25W	$7 \cdot 10^{9} W/m$	0.07 mW
Dual recycled 125W	$1.5 \cdot 10^{9} W/m$	0.08 mW

Table 1.5: Requirement on spurious field transmission through the OMC, assuming a residual intensity noise of 2%.

This in turn modulates the field inside the arms and induces an additional force on DARM via radiation pressure. The net effect is a reduced real motion of the degree of freedom. However, once the real displacement is properly computed, taking into account the depressing factor due to radiation pressure, the dark fringe power signal responds with a transfer function which depends only on the optics and corresponds to what one would get from computations which do not include radiation pressure.

The spurious DARM motion induced by a leakage field residual intensity noise is given by

$$\delta_{DARM} = \frac{P_s RIN_s}{G} \tag{1.8}$$

where G is the optical gain of dark fringe with respect to DARM; P_S is the total power of the leaking field and RIN_S is the corresponding residual intensity noise.

To properly control the DARM loop at the level of accuracy δz_{RMS} considered in the previous section, the contribution of spurious motion due to leaking field must be well below this level. If we ask this contribution to sum up to less than 10% of the needed accuracy, the limit on leaking field is given by:

$$P_S < \frac{1}{10} \cdot \frac{\delta z_{RMS} G}{RIN_S} \tag{1.9}$$

The resulting requirements on leaking power in transmission of the dark fringe are summarized in tab. 1.5 as a function of the interferometer configuration.

1.3.6 Design and performances of the control systems

The detailed iterative procedure to design a control scheme compatible with both the accuracy requirements and the noise re-introduction requirements is described in [6]. In each different configuration and for each degree of freedom, the error signal with highest signal-to-(shot)noise ratio has been selected and the corresponding demodulation phase tuned, see tab. 1.6.

To reduce the coupling of sensing noise to detector sensitivity below the safety factor, it was necessary to assume the implementation of noise subtraction paths [12] with performances of the order of a factor 500 of coupling reduction. This level is the one obtained in Virgo+ and it is considered feasible.

Moreover, during the control loop design it turned out that to achieve the desired accuracy it is necessary to properly diagonalize the sensing matrix. The precision needed for such diagonalization ranges from 10% in the power recycled case to fractions of 1% in the dual recycled case, which is a quite difficult performance to achieve. More investigations in this direction will be needed, in particular to assess the need of adaptive diagonalization of the sensing matrix. Very simple matrix diagonalization servos were already implemented in Virgo at the time of the first commissioning runs.

The performances in terms of accuracy are listed in tab. 1.6.

The level of control noise which is coupled to the detector sensitivity in the three configurations is shown in figure 1.3. The level of sensing noise is the one corresponding to shot-noise-limited sensitivity for 100 mW of total sensed power per auxiliary port. In all the configurations the MICH degree of freedom is the most critical and its control noise is at the limit of the factor 10 below design sensitivity.

The filter optimization is a balance between having high gain below 2-3 Hz to be able to reach the accuracy requirements and string enough roll-off at higher frequencies (above 10 Hz) to avoid re-introducing control noise in the detector sensitivity. The stability of the control loop imposes some limits on the possible optimization. The present design is barely fulfilling the requirements with the minimum acceptable stability margins (30 degree of phase margin and less than a factor 2 of gain margin). Further optimizations in the present scheme are not possible. Any increase of the sensing noise or of the payload motion would result in the longitudinal control being no more complaint with the design.

Another critical point is the implementation of the DARM loop in the dual recycled case. Indeed in this case the DARM opto-mechanical transfer function contains an unstable pole at some tens of Hz (the frequency is proportional to the input power). To stabilize the system it is therefore necessary to have a much larger band-width than in the Virgo+ case. The present design foresees a unity gain frequency of about 400 Hz, which is necessary to stabilize the system with suitable gain and phase margins and reach the required accuracy. The need of significantly increase the band-width of the DARM loop has strong consequences on the design of the real-time control system and of the payload. Indeed, the present design of the DARM loop is compatible with a total delay in the control chain of 50 μs (assuming the

Power recycled only at 25 W

D.O.F.	Error signal	Accuracy	Requirement
DARM	B1_DC	$5 \cdot 10^{-16}$ m	$6 \cdot 10^{-16}$ m
Frequency	B2_SB1_P	0.6 mHz	7 mHz
MICH	B4_SB1_Q	$1.3 \cdot 10^{-13}$ m	$2 \cdot 10^{-13}$ m
PRCL	B2_SB3_P	2×10^{-12} m	2×10^{-11} m

Dual recycled at 25 W

DOF	Error signal	Accuracy	Requirement
DARM	B1_DC	$1.1 \cdot 10^{-15}$ m	$1 \cdot 10^{-15}$ m
Frequency	B2_SB3_P	0.05 mHz	7 mHz
MICH	B4_SB2_Q	$1.8 \cdot 10^{-12}$ m	$2 \cdot 10^{-12}$ m
PRCL	B2_SB1_P	1×10^{-13} m	2×10^{-11} m
SRCL	B4_SB2_P	3×10^{-14} m	2×10^{-12} m

Dual recycled at 125 W

DOF	Error signal	Accuracy	Requirement
DARM	B1_DC	$6 \cdot 10^{-16}$ m	$1 \cdot 10^{-15}$ m
Frequency	B2_SB3_P	0.09 mHz	7 mHz
MICH	B4_SB2_Q	$2.4 \cdot 10^{-14}$ m	$2 \cdot 10^{-12}$ m
PRCL	B2_SB1_P	1×10^{-14} m	2×10^{-11} m
SRCL	B4_SB2_P	3×10^{-15} m	2×10^{-12} m

Table 1.6: Summary of error signals and obtained accuracies in: power recycled configuration at 25 W input power (top), dual recycled at 25 W (middle), dual recycled at 25 W (bottom).

phase margin must be larger of 30 degrees). This seems very difficult to achieve. On the payload design side, the structure that will hold the coils used to apply the control forces should not have structural resonances inside the active bandwidth of the loop, otherwise they could get too excited by the control itself. Having all structural resonances above 400 Hz seems very difficult. Both DAQ and PAY considerations triggered the need of a more deep study of the DARM control. It seems feasible to reduce the band-width to 200 Hz, even if a detailed design is not available yet. In this way the total delay requirement would be relaxed to 100 μs and the resonance requirement to 200 Hz.

More details on the final control system design are available in the note [6].

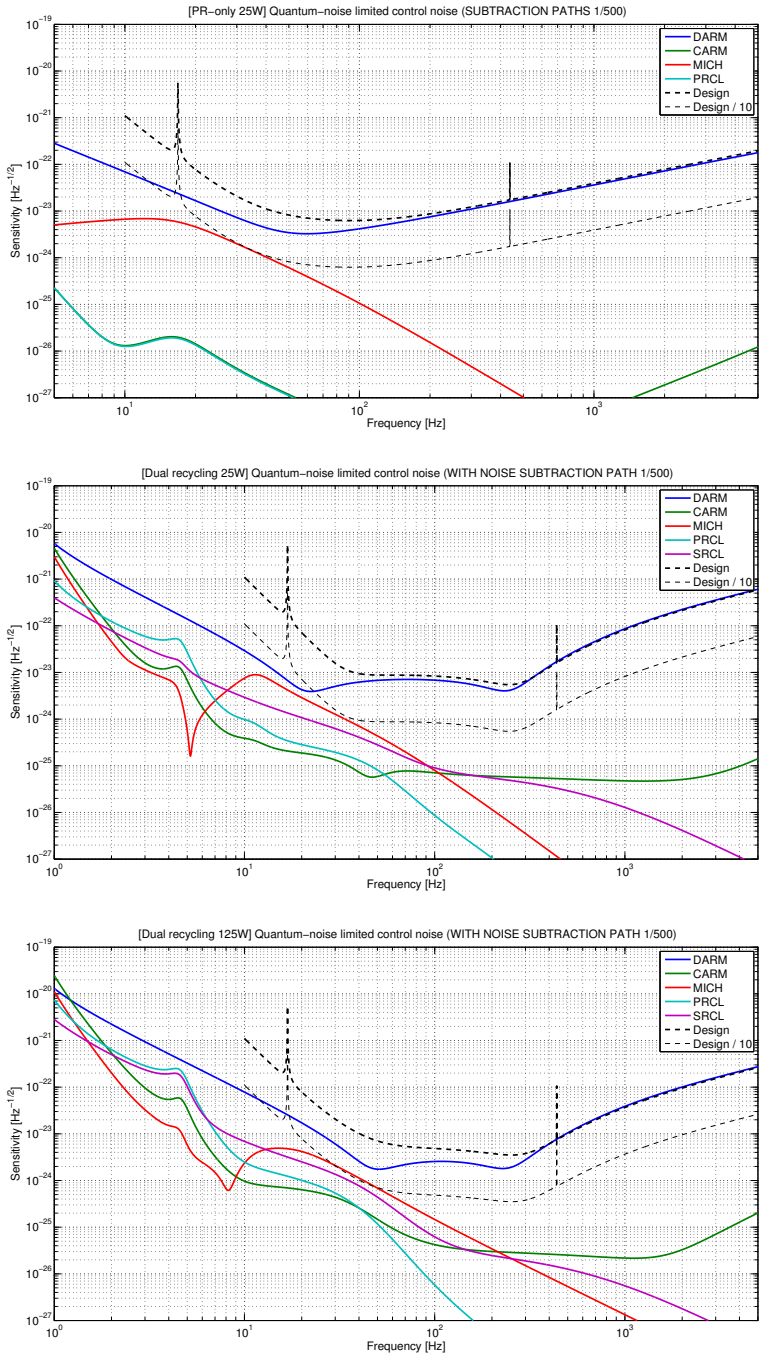

Figure 1.3: Sensing noise re-introduced in the detector sensitivity by longitudinal control loops in the three configurations: power recycled only with 25 W input power (top), dual recycled with 25 W input power (middle), dual recycled with 125 W input power (bottom).

1.3.7 Requirements on modulation and demodulation noises

The main gravitational channel is extracted using DC readout, therefore it is not affected by radio-frequency sideband noises, provided the OMC filtering is adequate. However all the signals used for the auxiliary degrees of freedom control are obtained with a standard demodulation technique. Therefore any phase or amplitude noise of the radio-frequency sidebands will pollute these signals.

The coupling of phase and amplitude noise can be modeled with good accuracy as a cross quadrature coupling [13]. If the Q quadrature of a signal is not perfectly zero, due to an offset or to residual RMS motion, it induces a coupling of phase noise to the P quadrature. A similar coupling exists for the sideband amplitude noise, this time coupling each quadrature with its own RMS motion. The two couplings can be described using the following equations:

$$\tilde{n}_P(f) = \delta Q_{RMS}\, \tilde{\phi}(f) \tag{1.10}$$

$$\tilde{n}_P(f) = \delta P_{RMS}\, \frac{\tilde{\delta A}(f)}{A} \tag{1.11}$$

where $\tilde{\phi}(f)$ is the spectrum of the phase noise measured in rad/$\sqrt{\text{Hz}}$, $\frac{\tilde{\delta A}(f)}{A}$ is the residual amplitude noise of the sideband at the given frequency measured in $1/\sqrt{\text{Hz}}$, δP_{RMS}, and δQ_{RMS} are the residual motion or offset in the P or Q quadrature. Finally $\tilde{n}_P(f)$ is the resulting noise into the P quadrature. Similar equations hold for the other quadrature.

From the simulations described in the previous sections, the obtained loop accuracy can be translated in residual RMS signals in each port quadrature. Asking the sideband phase and amplitude noise to be a factor 10 below the shot noise, one can obtain requirements on the total modulation and demodulation noises at the mixer input. Results are summarized in tab. 1.7, quoting only the most stringent requirement for each frequency, regardless of the interferometer configuration. Refer to [INJ chapter, section 1.6.4] for a comparison with the expected performances.

1.3.8 ITF asymmetries and coupling of laser noises

In order to assess requirements for power and frequency noises, Optickle was used to simulate Advanced Virgo interferometer in two configurations: power recycled at 25 W and dual recycled at 125 W.

As well known, Optickle has some limitations, in particular it cannot deal with higher order modes other than the first one, so it cannot be used to evaluate the effect of geometrical asymmetries such as arm length and/or

Frequency	**Phase noise** [**rad**/$\sqrt{\textbf{Hz}}$]	**Rel. ampl. noise** [$1/\sqrt{\textbf{Hz}}$]
6.3 MHz	$1.8 \cdot 10^{-6}$	$1.7 \cdot 10^{-7}$
56.4 MHz	$1.1 \cdot 10^{-6}$	$1.1 \cdot 10^{-6}$
8.4 MHz	0.27	$1.7 \cdot 10^{-7}$

Table 1.7: Summary of requirements for sideband amplitude and phase noise. Modulation noises enters in the photo-diode output signal following two paths. The first one is through the noise at the level of the modulation, which is transmitted to the laser beam and enters on one of the inputs of the mixer. The second path is through noise introduced by the local oscillator distribution system, which enters on the other input of the mixer. The requirements given here apply to the total of the two contributions.

radius of curvature mismatch, and it cannot even handle figure error maps for the core optics. On the other hand, it is possible to include radiation pressure effects and mechanical transfer functions, that are important at low frequency. Simulations were then carried out in order to evaluate the effects of loss and finesse asymmetries on the coupling of laser power and frequency noises to the dark fringe and the impact on Advanced Virgo sensitivity. Although possible, no control loops were included in the simulation so to speed up calculations.

Power recycled configuration at 25 W

Starting from a situation without any defect, finesse and loss asymmetries were introduced one at a time and together [14, 15]. Frequency noise requirements are reported in fig. 1.4 both for the no defect case and for some values of finesse and loss asymmetries. Without SRC and without any defect, the requirements for frequency noise are much more relaxed with respect to the dual recycled configuration, but they worsen very quickly as soon as defects are introduced in the simulation. For this configuration loss asymmetry is the worst offender at high frequency, and finesse asymmetry at intermediate frequency.

The situation is more complicated for the power noise requirements (see fig. 1.4), as for the coupling to the detector sensitivity also the sign of the asymmetries plays a role, but in general we have almost a factor 10 less coupling for power recycled only with respect to dual recycled.

Dual recycled configuration at 125 W

Starting from a situation without any defect, finesse and loss asymmetries were introduced one at a time and together [14, 15]. It turned out that loss

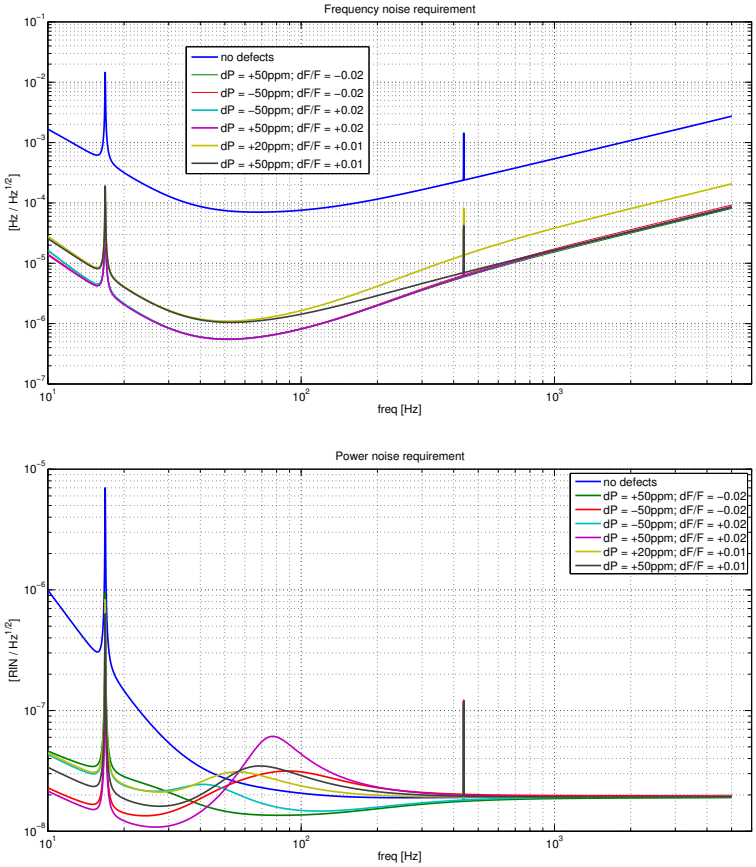

Figure 1.4: Laser and frequency noise requirements for power recycled at 25 W configuration, a safety factor of ten has been used to draw the requirements from nominal sensitivity. Different values of finesse and loss asymmetries have been used. Top: laser frequency noise at interferometer input. Bottom: laser intensity noise at interferometer input.

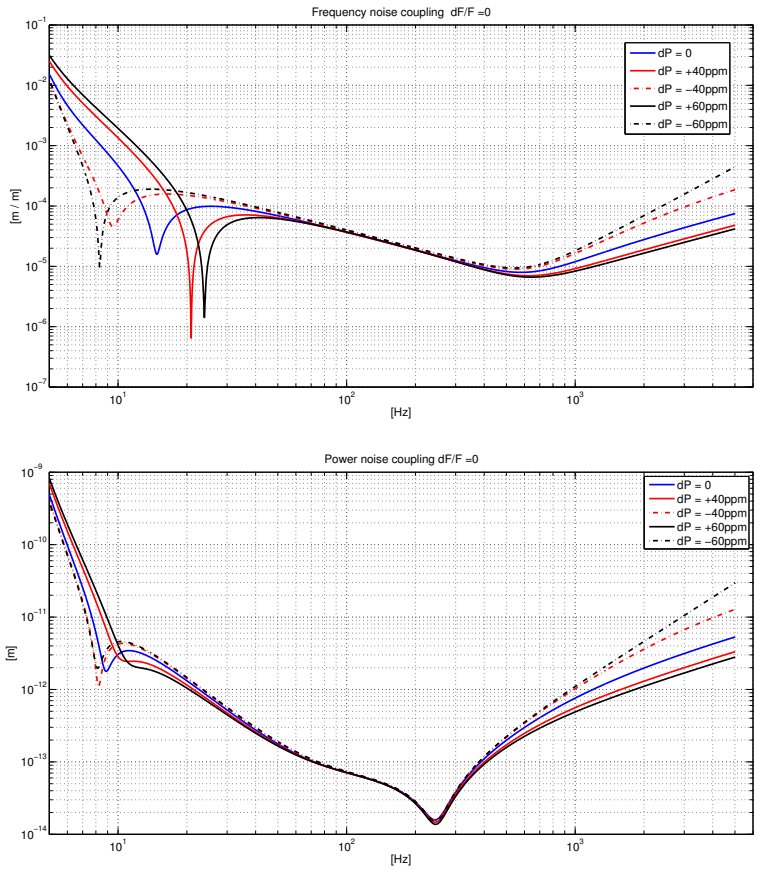

Figure 1.5: Dual recycled at full power configuration. Transfer functions in case of equal finesse (F = 443) as a function of round trip loss asymmetry. Average round trip losses are 75 ppm. Top: frequency noise transfer function. Bottom: power noise transfer function.

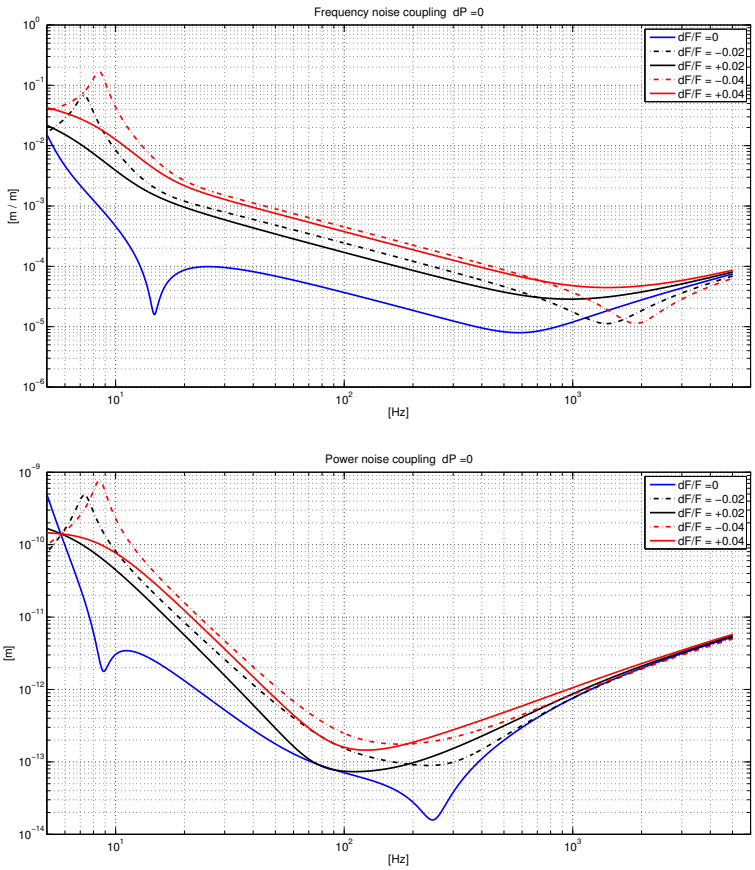

Figure 1.6: Dual recycled at full power configuration. Transfer functions in case of equal round trip losses (RTL = 75 ppm) as a function of finesse asymmetry. Average finesse is 443. Top: frequency noise transfer function. Bottom: power noise transfer function.

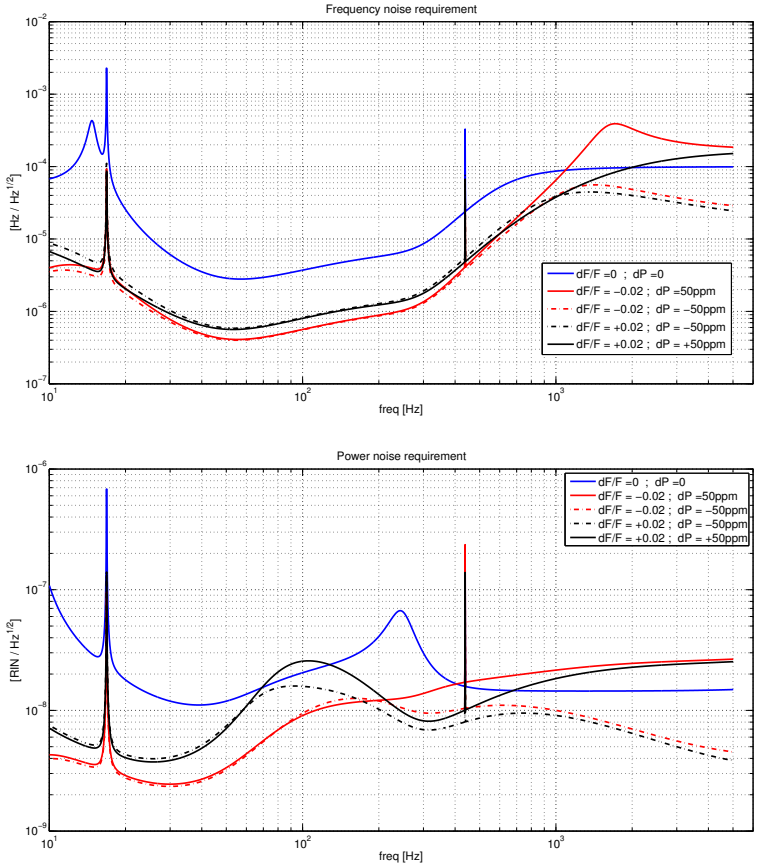

Figure 1.7: Dual recycled at full power configuration, frequency and power noise requirements with a safety factor of ten used to draw the requirements from nominal sensitivity. Different values of finesse and loss asymmetries are used. Top: laser frequency noise at interferometer input. Bottom: laser intensity noise at the interferometer input. Blue curve: no defects. Red curves: dF/F = -2%; black curves: dF/F = +2%. Solid curves: dP = +50 ppm, dashed curves: dP = -50 ppm.

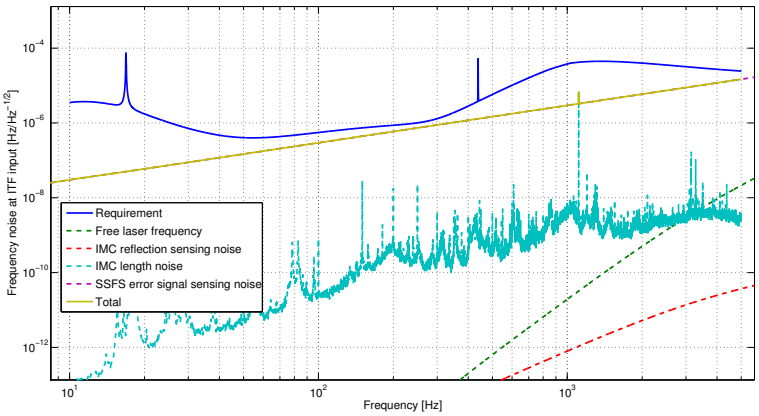

Figure 1.8: Contribution of different noise sources to stabilized laser frequency at the interferometer input, in the dual recycled configuration at full input power (125 W).

asymmetry is the worst offender at high frequency (see top plots of figures 1.5 and 1.6), while finesse asymmetry plays more a role at intermediate frequency (see bottom plots of 1.5 and 1.6), for the coupling of laser power and frequency noises to DARM. One important thing to notice in those plots is that asymmetries are not symmetrical: the sign does play a role in shaping the coupling of laser noises to DARM, depending on the sign set to the DARM offset, and this could make choosing the sign of this offset a bit tricky, as a situation could occur where the signs of asymmetries require contradictory optimizations with respect to DARM offset sign. Based on those simulations, requirements on input technical noises are drawn considering several combinations of signs for the aforementioned asymmetries (see fig.1.7, and files attached to [15]).

Triggered by a proposal put forward by DET subsystem [16], frequency and power noise couplings are also recomputed with an increased offset on DARM degree of freedom. The aim was to check whether doubling the offset would have had a negative impact on those noise couplings, but as far as only finesse and loss asymmetries are concerned (no other defects introduced in the simulation), there are no dramatic changes in frequency and power noise couplings to sensitivity.

1.3.9 Second stage of frequency stabilization

The second stage of frequency stabilization (SSFS) is used to lock the laser frequency to the arm cavity mean length. It is necessary to meet the re-

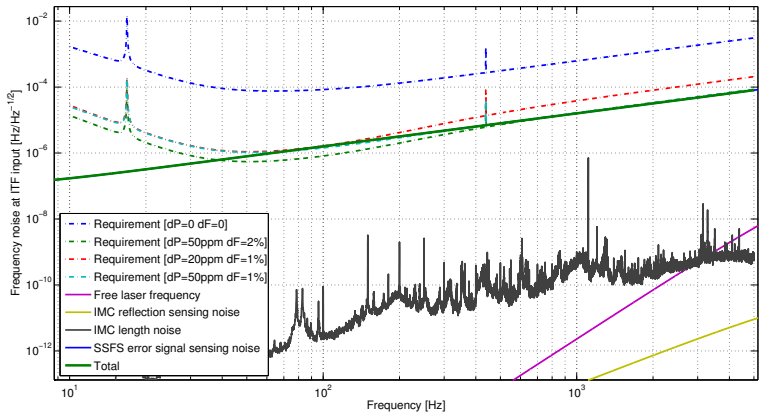

Figure 1.9: Contribution of different noise sources to stabilized laser frequency at the interferometer input, in the power recycled configuration at 25 W input power.

quirement on residual frequency noise detailed in sec. 1.3.8. The control architecture is the same as in the Virgo+ case: the correction computed by the SSFS controller is added to the error signal of the laser frequency prestabilization and simultaneously used for the lock of the input mode cleaner [17]. The error signal which will be used is always extracted from the interferometer reflection, demodulated at f_1 or f_3 depending on the optical configuration.

The unity gain frequency of the SSFS loop is expected to be at about 20-30 kHz, the upper limit set by the arm cavity free spectral range notch. Controllers with such a high bandwidth are easily built using analog electronic, as done in Virgo+. However it is known that the shape of the interferometer optical transfer function between 3 and 50 kHz depends strongly on sidebands aberrations. The possibility of using an ad-hoc digital control system with high sampling rate is being investigated. This would provide the needed flexibility to cope with changes in the optical transfer functions, without the need of re-building the analog electronics every time the interferometer behavior changes.

A detailed design of all the paths involved in the full frequency stabilization system has been done [18] and the performances compared with the requirements of sec. 1.3.8. When the laser frequency is stabilized on the interferometer reflection, the limiting factor in the performance is, as expected, the shot noise of the SSFS error signal. In the dual recycled case the level of frequency stability meets the requirements even in presence of relatively large interferometer asymmetries (50 ppm of losses asymmetry and

2% of finesse asymmetry), see fig. 1.8. The power recycled case is instead more critical, see fig. 1.9: losses asymmetries must remain below 20 ppm and finesse asymmetry below 1% to be able to meet the requirements.

1.3.10 Input mirror Etalon tuning

As explained in the previous section, in the power recycled case it is necessary to maintain the finesse asymmetry below 1% in order to meet the requirement on frequency noise coupling to the detector sensitivity. During Virgo commissioning the ability to minimize the coupling of common noises at low frequency has been extensively used and proved crucial to reach good detector sensitivity. The noise sources that coupled proportionally to the finesse asymmetry were only partially identified (frequency noise, limited by the sensor shot noise, and input beam jitter). There remained several noises which source was not identified, since it was possible to largely reducing their coupling to the detector sensitivity by fine tuning the finesse of the two arms.

For these reason it is proposed to implement input mirrors with parallel faces, in order to be able to fine tune the finesse asymmetry in a continuous way during the interferometer operations. The plan for Advanced Virgo would be to stabilize the input mirror temperature with slow servo systems. They will use heaters attached to the vacuum towers which will then act as a thermal bath for the input mirrors. This technique has already being tested successfully in Virgo. The needed range of finesse change is under study and will be decided as soon as more detailed simulations will be available.

1.4 Longitudinal control system: lock acquisition

The Advanced Virgo lock acquisition can be divided in mainly three almost decoupled parts. The first is the lock acquisition of the arm cavities, as stand-alone configuration or as the first step of the full interferometer lock. The second part is the lock acquisition of the interferometer in power recycled configuration. Finally the last part is the lock acquisition of the full dual recycled interferometer.

1.4.1 Lock acquisition of the arm cavities

One of the main differences of Advanced Virgo with respect to Virgo+ is the increase of the finesse of the arm cavities from around 150 to 443. As a result of this, the maximum velocity of the mirrors below which the lock

can be acquired will be much lower. This will increase the time needed to lock the cavities or might even make it impossible to lock. One strategy which was tested many years ago at LIGO and TAMA is to first measure the velocity once the cavity sweeps through a resonance and then apply a long rectangular pulse to bring it back to resonance with reduced velocity. Once the velocity is reduced enough, the cavity can be locked with a standard linear feedback loop.

Such strategies have been tested experimentally just before the shut-down of Virgo+ with good results. It was even possible to lock the cavities with a force that was 160 times lower than the maximum available force, see fig. 1.10. One important observation was that to keep the cavity locked with low force for more than a few seconds, it is necessary to immediately reallocate the low-frequency part of the correction to the marionette actuators.

Similar tests were done in simulation using the optical parameters of Advanced Virgo, see fig. 1.11. They show that the scheme should still work for the optical properties of the future cavities. Still missing from the simulation are an accurate representation of the mechanics and the noise in the detection process. The exact noise-level that can be tolerated has still to be determined.

These results indicate that, even with the increase in finesse, the strength of the magnets glued to the mirrors might be reduced somewhat. This is very desirable for reducing the coupling of environmental magnetic noise and for simplifying the design of the payload. How much the magnets can be reduced can only be decided once the design of the new payload is known. More details are given in a separate Virgo-note [19].

1.4.2 Lock acquisition in power recycled configuration

In this section the lock acquisition technique proposed for Advanced Virgo in the power-recycled configuration is shortly described. It is very similar to the one used in Virgo+ during the last science run VSR4, which is called the *variable finesse* technique [20].

Arm cavity lock. In order to decrease thermal effects, the idea is to start the lock procedure with low input power and to increase it once the interferometer is steadily locked. The initial state of the uncontrolled interferometer is with all the mirrors roughly aligned except the power recycling mirror (PR), which is misaligned so that its reflection does not return towards the beam-splitter to form a cavity. At the beginning of the lock procedure the two arm cavities are independently locked using the in-phase demodulated signals in transmission with a standard Pound-Drever-Hall (PDH) technique, which are normalized by the powers transmitted by

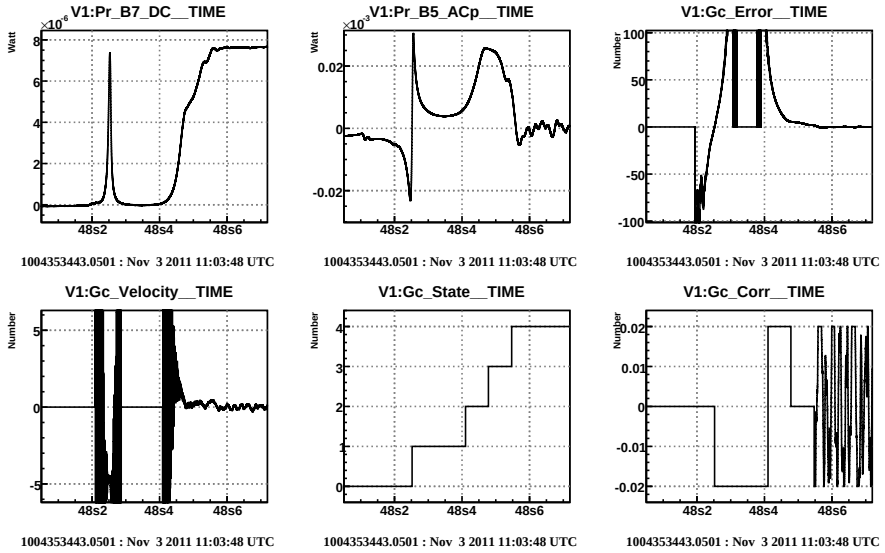

Figure 1.10: Experimental demonstration using Virgo+ of a lock with reduced force implemented in Gc. The reflection error signal is normalized with the power transmitted by the cavity. The velocity as the derivative of the error signal. Two pulses with opposite sign are applied. The lengths of the two pulses are calculated to bring the mirror back at resonance with velocity zero and are proportional to the velocity measured while crossing the resonance. The logic is implemented as a state-machine (0 = wait for resonance, 1 = first pulse, 2 = second pulse, 3 = wait for return to resonance, 4 = linear lock). The lock was acquired with a maximum correction of 0.02 Volt on 1 coil-pair, while a maximum of 0.8 Volt on 4 coil-pairs is available.

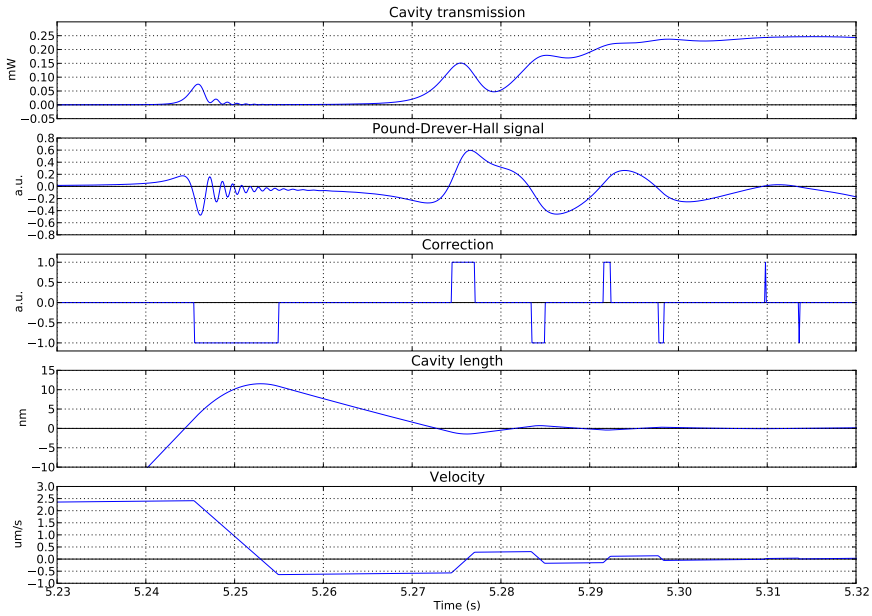

Figure 1.11: Lock acquisition of an Advanced Virgo arm-cavity, as simulated with e2e. Note that the cavity length and velocity are properties that are only available in simulation and cannot be observed directly in reality. They are normally estimated, as described in the caption of fig. 1.10 as the derivative of the error signal on resonance crossing.

the cavities in order to increase the linear range of the error signals.

The lock of the cavities is obtained by applying small forces to the mirror, with the coils assembled on the cage connected to the filter 7 of the super-attenuator. When the lock is reached, the longitudinal correction applied to end and input mirrors is reallocated to the marionette actuators, as described in sec. 1.4.1. Due to the very different amount of power during the lock procedure, two different photo-diodes could be needed to detect the transmitted light by the end mirrors: one for low power at the beginning of the procedure and the other for high power in steady state.

Half fringe lock. At the dark port, the resonance condition is initially chosen to be at half fringe (half of the maximum possible power is transmitted), which is outside the linear range of the demodulated signal. A method using the DC powers is therefore used to lock the MICH degree-of-freedom: the ratio of the power transmitted to the dark port over the power impinging on the arm cavities (read with the PR pick-off beam) gives an estimation of the Michelson fringe value. The fringe offset is set to 0.5 at the beginning, which is a standard side-of-fringe locking of a Michelson interferometer and does not depend on any optical parameter of the cavities. The lock-acquisition of the MICH loop is thus virtually identical to the one used for initial Virgo.

Frequency stabilization. After these first steps, in Virgo and Virgo+ the control strategy of the two arms is modified. The SSFS, which keeps the laser frequency locked to the mean length of the arms below some tens of kHz (see 1.3.9 and [18]) is engaged. The control of DARM is made by exploiting an error signal given by the transmission of one of the two cavities. The CARM control is instead implemented using an error signal from the Reference Cavity (RFC) reflection with about 1 Hz of band-width: in this way the low frequency residual motion of the end mirror and of the laser frequency are reduced to a suitable value (see also sec. 1.3.4 for CARM accuracy requirements).

In the Advanced Virgo case the error signal foreseen for the SSFS comes from the interferometer reflection (see sec. 1.3.6) and it is not available before the PR is aligned. It might be necessary therefore to modify the described strategy: the SSFS could be engaged after the re-alignment of the PR (this was done in Virgo at the time of the first commissioning runs) or it could use a different error signal for the lock acquisition (like B4 as done in Virgo and Virgo+) and switch to the final signal later.

PR re-alignment. At this point of the lock acquisition, the PR is re-aligned. During this transition the circulating power inside the interferometer increases by a large amount. Therefore all the signals are subjected to a large change in their optical gain, which is compensated by the use of suitable normalization. At the same time the longitudinal control of the PR

	Misaligned PR	Aligned PR	Science Mode
MICH Offset [m]	$1.33 \cdot 10^{-7}$	$1.33 \cdot 10^{-7}$	$1.60 \cdot 10^{-9}$
B1p [W]	$2.45 \cdot 10^{-2}$	$2.41 \cdot 10^{-1}$	$8.34 \cdot 10^{-3}$
B2 [W]	$1.22 \cdot 10^{-3}$	$7.48 \cdot 10^{-1}$	$1.61 \cdot 10^{-1}$
B4 [W]	$1.50 \cdot 10^{-5}$	$1.48 \cdot 10^{-4}$	$1.14 \cdot 10^{-2}$
B7 [W]	$6.91 \cdot 10^{-6}$	$6.82 \cdot 10^{-5}$	$5.28 \cdot 10^{-3}$
Arm power [W]	6.91	$6.82 \cdot 10^{1}$	$5.28 \cdot 10^{3}$

Table 1.8: DC powers of various output ports during the lock-acquisition, for 1 Watt of input power. Arm cavities are always locked. Note that in the real interferometer B1p power will depend strongly on contrast defect and higher order mode contents.

is engaged using an error signal normalized by the value of the power inside the recycling cavity. Note that the finesse of the recycling cavity is in this configuration dominated by the loss of the short Michelson interferometer at half-fringe. The lock-acquisition of the PRCL loop should thus be virtually identical to the one used in Virgo and Virgo+. This is the first condition of the interferometer with all mirror aligned and all longitudinal degrees of freedom controlled.

MICH offset reduction. The locking point of the MICH loop is finally moved in several steps towards its final value, which is close to the dark fringe, see sec. 1.3.3. During this transition the power in the cavities increases by about a factor 100 and gains of the lock loops have to be changed accordingly. An analysis of the different condition in lock-acquisition procedure has been carried out using the simulation tool e2e [3]. In table 1.8 the calculated values for the DC power of various output ports during the lock-acquisition for 1 W of input power are shown. The large excursion of the power impinging on the diodes might require the use of switchable sets of electronic gain.

Reaching dark fringe. The DARM loop control is then switched to a demodulated signal coming from the beam extracted before the OMC (B1p). The automatic alignment for the all degrees of freedom is engaged.

OMC and low noise configuration. The procedure that put the OMC in resonance is then started and the DARM loop control is finally switched to the DC-readout signal in transmission of the OMC (B1). At this point the interferometer is locked in a robust configuration and the operating point is very close to the final one. When the interferometer is in a steady condition, the input power is increased to the final value. When all the thermal effects connected to the increase of the input power are stabilized, the control filters of all the longitudinal and angular degrees of freedom are optimized in order to reduce control noise below the requirements. All the actions performed

at the end of the lock acquisition procedure are focused to improve as much as possible the sensitivity of the detector (for example engaging of noise subtraction paths, etc.).

As explained in sec. 1.3.3, we do not expect large effects due to radiation pressure in the power recycled configuration, provided the idea of putting the DC-readout offset on MICH is feasible as shown in simulations.

1.4.3 Lock acquisition in dual-recycled configuration

So far the lock-acquisition of Advanced Virgo in the dual recycled configuration has not been studied yet. One possible solution would be to follow the strategy employed by LIGO, which is briefly explained here. The idea is to first lock the arm-cavities using an auxiliary laser, with a technique similar to the one described in the next section 1.5. After this, the lock is transferred to the main laser, using an error signal calculated from the DC signals in transmission of the cavities. A very large offset is applied to the CARM degree of freedom, so that the cavities are almost out of fringe. In this condition, the PRCL and SRCL degrees of freedom are locked. Finally, the offset is adiabatically removed. During this transition, the opto-mechanical resonance of the interferometer shifts in frequency, causing large changes in the optical transfer-functions. It appeared that the signals of the central interferometer demodulated at 3 times the modulation frequencies are more robust during this transition, since they depend more on the resonance condition of the sidebands, than on the carrier that resonates in the arm-cavities [7].

An alternative method might be to extend the current *variable finesse* technique to the lock of the SRCL degree of freedom. The idea would be to first lock the two arm-cavities with both the PR and SR misaligned, lock MICH at half-fringe and then align both mirrors one at a time. Finally, the offset of MICH would be adiabatically moved towards the dark-fringe.

The lock acquisition strategy for the dual recycled interferometer is at this stage not a high priority task, since it is expected that during the first commissioning phases the Advanced Virgo detector will run in power recycled configuration. Nevertheless the study of the lock acquisition in dual recycled configuration will start in the next months and first results are expected at the beginning of the next year.

1.5 Auxiliary lasers

1.5.1 Goals of the auxiliary lasers

The use of auxiliary lasers was first proposed to lock the very high finesse (1200 and then 900) long cavities in the Advanced Virgo design. The idea is to use an auxiliary laser at a wavelength far from 1064 nm so that the finesse seen by it can be chosen independently of the one seen by the main laser. A low finesse (typically lower than 10) makes the lock of the cavity easy and allows to control its length down to a nm precision. It is then sufficient to change the working point of the lock (or the frequency of the laser) to be able to cross a resonance of the main laser and then switch to the latter one for the full control.

With the current finesse for Advanced Virgo (443), it has been shown that even if we reduce the actuator maximum forces by a factor 5 (with respect to Virgo+ during the lock acquisition) we can still lock the long arm cavities with the main laser [21] using a Virgo-like technique. Therefore, as explained in sec. 1.4.2, the lock acquisition strategy in the power recycled configuration will be very similar to the Virgo one and there will be no need of auxiliary lasers.

However we will still face the problem to lock the interferometer with the presence of the signal recycling mirror, which will increase the complexity to acquire the lock. As explained in the previous section, the lock acquisition will be eased if we can have the long cavities frozen but off-resonance from the main laser. Such action could be performed with an auxiliary laser as long as we can control the long cavities without getting the main laser resonating in the arms during the five minutes planned for the lock acquisition of the central interferometer.

Therefore the design and integration of the auxiliary laser system in Advanced Virgo can be break down in two steps. The interferometer must be designed in order to be compatible with the system as explained in the next sections, but choosing the correct mirror coating and foreseeing the room of optical benches. If needed and useful, the actual installation could take place only in a second time, when Advanced Virgo will move from power recycled to dual recycled operations.

1.5.2 Implementation and requirements

The present plan is to inject two independent auxiliary lasers from the end station benches. The optical tables will be placed close to the mini towers and on the same concrete slabs. Depending on the telescope design, the

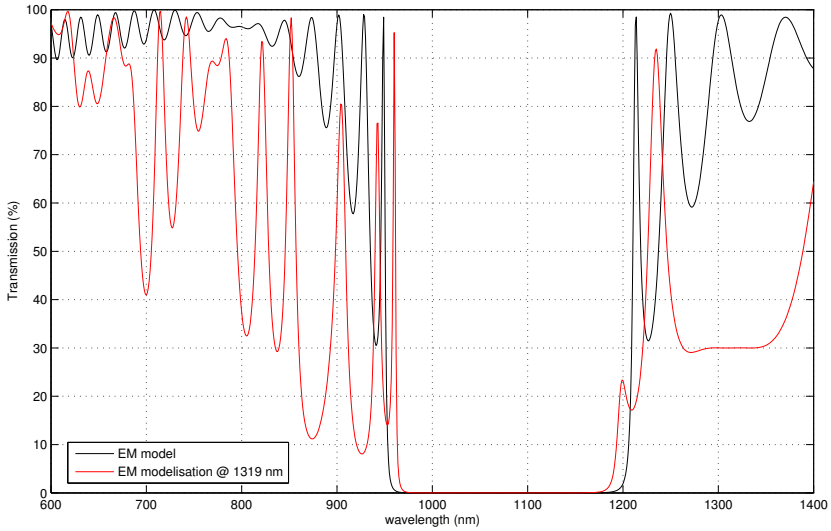

Figure 1.12: Advanced Virgo end mirror transmission model depending on the wavelength. Two models are presented: the current one (black curve) and a possible modification to provide low finesse at 1319 nm. The optimization has been done by LMA to keep the same transmission at 1064 nm and to avoid too much layers on the coating. The new coating have been studied to reduce at maximum the number of layers: between the two designs the width of the coating will be changed by 300 nm (on a total of 7 μm). The impact on thermal noise is expected to be negligible.

optical table may be shared with the Hartman beam. The different optics on this table will be used to control the beam position and to adapt it to the end arm telescope.

The choice of wavelength is driven mainly by the mirror reflectivity we can have without changing the one planned for the 1064 nm, to obtain a low finesse cavity, see fig. 1.12. The Nd-YaG solid state laser at 1319 nm seems to satisfy the different requirements and gives a free running low frequency noise.

If we want to lock the cavity on the auxiliary laser a frequency stabilization loop will be however needed. This could be achieved by using a reference cavity on the optical table like the one used on the injection bench. The requirements also need to take into account that we do not want to cross a 1064 nm resonance during 5 minutes while we are locked on the auxiliary laser. Some simulations were performed to assess the frequency stability for the auxiliary laser using a simple Fabry-Perot cavity in Siesta. The frequency noise spectrum is the one from Virgo given in figure 23 of [22] for

the 1064 nm. The same spectrum has been used for the auxiliary laser. To this noise we also added a long thermal drift (30 Hz/s) as reported in [17]. Such a preliminary work showed that even by multiplying the frequency noise of the auxiliary laser by more than a factor 10 the goal can still be achieved.

We think we can use two lasers with the same wavelength for the two arms and select a different polarization for each of them. Then a polarizer will be needed for all photo-diodes used in the system. The design of the optical table is currently under study. The system will be a standard one with laser and optics to select the polarization, a pick-off towards the reference cavity, an Electro-optical modulator (EOM), a telescope to match the beam to the end arm detection table and some motorized optics for alignment. We will use a set of photo-diodes to control the lasers (power and frequency) and the long cavity by using the reflected beam. We will also control the position and alignment of the beam with some quadrants photo-diodes. The loops to control the laser will be done locally. The control of the cavity will be performed directly in the locking algorithm of the global control system.

When the lock acquisition procedure will be completed, we will switch off the auxiliary lasers to avoid any perturbation to the detector in Science Mode.

The auxiliary lasers will not be needed before the installation of the SR and so their installation can be delayed up to that time. The different interactions with the MIR, DAQ and DET subsystems have been defined and taken into account in their designs. The installation could be done in two steps. We could start to construct the in-air optical table independently and characterize the beam and the different optical elements. This phase may be done in LAL before bringing the elements on site. Otherwise we could start the installation in the end-arm station. Finally we will need to have access to the long cavities to align the beam correctly for at least one month per arm.

Most of the requirements and techniques will be tested on the CALVA platform under commissioning in the Laboratoire de l'Accelerateur Lineaire.

1.6 Sideband aberration risk reduction strategy

Simulations of thermal effects and mirror surface and substrate defects in the power recycling cavity showed a large sensitivity of radio-frequency sidebands. Very large aberrations can degrade significantly the quality of the longitudinal error signals. The thermal compensation system is designed to be able to measure and compensate these effects. However it is important, at least in the first stages of commissioning, to have a strategy to robustly

control the interferometer even in presence of strong sideband aberrations.

Modal and FFT simulations show that the sideband sensitivity to PRC defects depends on their recycling gain. The larger it is the more sensitive the sidebands are to defects [8]. For this reason an additional modulation frequency of 21 times the first one $f_4 = 131.686317$ MHz will be used. The corresponding sideband will have a recycling gain of few units and will be poorly sensitive to PRC defects.

Signals from this additional modulation frequency will be needed at all central part ports and they will be used to control the interferometer in the first steps of commissioning of the thermal compensation system. The modulation depth could be smaller than the one of the main modulation and the photo-diode requirements in term of demodulation noise and efficiency could be relaxed, since these signals will be used during the lock acquisition stage when noise performances are not critical.

1.7 Angular control system

1.7.1 Introduction

In order to ensure long data taking periods the interferometer has to be kept on the chosen working point, this means, among other things, that the core mirrors have to be aligned with respect to the beam. So a global angular control system or automatic alignment (AA) system has to be implemented.

The main differences between the Advanced Virgo and the Virgo interferometer configurations are the higher circulating power and the presence of the signal recycling cavity. These modifications produce an improvement in the interferometer sensitivity but an increase of complexity for the development of the AA control system:

High circulating power: the high amount of laser power produces strong radiation pressure effects, as it will be detailed in sec. 1.7.2, which modify the mechanical transfer functions of the angular degrees of freedom.

Presence of the signal recycling cavity: it adds to the number of degrees of freedom to control and further increases the off-diagonal couplings in the AA error signals.

The AA control system has been fully designed in the three configurations already described in the introduction: power recycled only at 25 W, dual recycled at 25 W and 125 W.

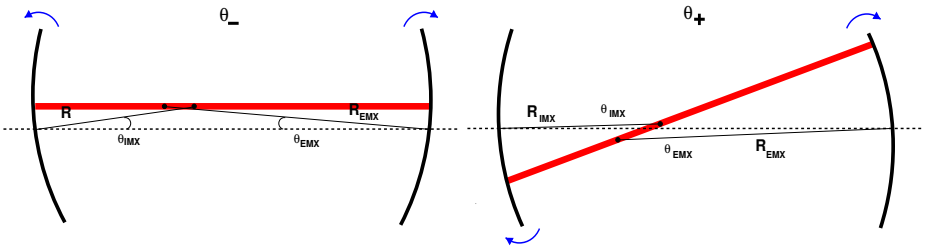

Figure 1.13: Effect of radiation pressure in a Fabry-Perot cavity. The two mirror modes become connected by an optical spring. The Fabry-Perot cavity mis-alignments can be described using the (+) *plus* and (-) *minus* modes. The combinations of single mirror mis-alignments giving the two modes depend on the cavity geometry.

The design consisted in the definition of accuracy requirements (the maximum allowable mis-alignments which do not affect the interferometer performances) and the development of the sensing and control scheme, including the evaluation of control noises.

This analysis has been carried out using the simulation tools *Finesse* [1] and *Optickle* [2].

Finally requirements for other sub-systems are given: quadrant photo-diodes specifications (quantity, demodulation frequencies, etc ...) and suspension requirements for the terminal detection benches.

1.7.2 Radiation pressure effect and angular modes

In a high power interferometer radiation pressure plays an important role. The laser beam acts on the mirror with force proportional to the power. The largest effect is present in the long arm Fabry-Perot cavities, since there the highest amount of laser power is stored, but the effect has to be also evaluated on the central interferometer mirrors.

It is possible to analytically compute the radiation-pressure modes using the system energy equations, based on the Sidles-Sigg small angle propagation [23]. On the other hand the effects can be simulated numerically using Optickle. The eigen-vectors of the system are the (+)-mode (the eigen-frequency increases depending on the cavity g parameters and on the radiation pressure, making the mode stiffer), and the (-)-mode (the eigen-frequency decreases making the system softer). The resonant frequency for the (+)-mode increases as the square root of the input power reaching ap-

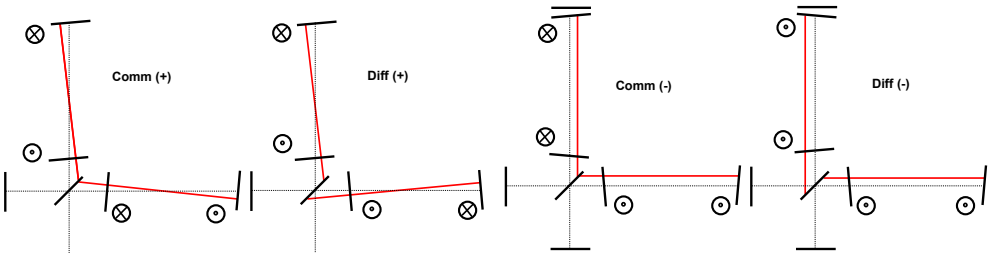

Figure 1.14: Graphical description of the physical modes for the Advanced Virgo interferometer in the yaw direction. Considering the direction of rotation referred to the front side of the optical component defined by the high-reflective coating.

proximately 3.5 Hz at full input power (125 W). The lower eigen-frequency, the (-)-mode, decreases smoothly to 1.1 Hz, remaining stable.

The central interferometer angular degrees of freedom are not significantly affected by radiation pressure due to the low amount of power impinging on the mirrors, see [24].

The single arm cavity angular motions will be described using the physical (+) and (-) modes base. When the entire interferometer is considered, the physical angular degrees of freedom are combinations of the central interferometer and arm cavity mirror mis-alignments:

- **Central interferometer degrees of freedom**
  - PR power recycling mirror
  - SR signal recycling mirror
  - beam splitter (BS), beam splitter mirror
- **Long arm degrees of freedom**
  - Comm(+) $= \frac{(-\alpha\,\mathrm{NI}+\beta\,\mathrm{NE})\pm(\alpha\,\mathrm{WI}-\beta\,\mathrm{WE})}{2}$
  - Comm(-) $= \frac{(\beta\,\mathrm{NI}+\alpha\,\mathrm{NE})\pm(-\beta\,\mathrm{WI}-\alpha\,\mathrm{WE})}{2}$
  - Diff(+) $= \frac{(\alpha\,\mathrm{NI}-\beta\,\mathrm{NE})\pm(\alpha\,\mathrm{WI}-\beta\,\mathrm{WE})}{2}$
  - Diff(-) $= \frac{(\beta\,\mathrm{NI}+\alpha\,\mathrm{NE})\pm(\beta\,\mathrm{WI}+\alpha\,\mathrm{WE})}{2}$

where α=0.6470 and β=0.7625 depend on the cavity geometry, and the $\pm$ are for the yaw (θ_y) and pitch (θ_x) directions respectively, the change of sign is due to the reversing reflection of the beam splitter mirror. Fig. 1.14 shows a scheme of these degrees of freedom for the yaw direction.

d.o.f.	**req. [nrad]**	**d.o.f.**	**req. [nrad]**
(+)-mode	2	(-)-mode	110
PR	25	SR	280

Table 1.9: Angular requirements for the Advanced Virgo optical configuration in the physical mirror modes base.

1.7.3 Accuracy requirements

The angular accuracy requirements for the advanced Virgo mirrors have been evaluated for the arm cavity mirrors, the SR and the PR [25]. Since the mirror radii of curvature are of the order of one km the vertical and horizontal mirror displacement requirements are very easily fulfilled.

The RMS accuracy requirements of the cavity mirrors alignment are set in order to have acceptable fluctuations for the carrier and the sidebands power in the cavities, smaller than 10^{-3} relative [26, 27]. For the SR the requirements has to be set in order to do not vary the sensitivity more than a factor 10^{-2} in the whole detection frequency band. Results are given in tab. 1.9. These requirements are achievable with present Virgo alignment techniques. For example since VSR1 the Differential-End pitch and yaw d.o.f. were controlled with few nrad of accuracy [28, 29]. Moreover the relatively loose requirement on the SR alignment accuracy allows a low frequency control (i.e. the Virgo *Drift Control* [29] with tens of mHz of band-width and typical accuracy of 100 nrad) which is simpler to implement even in presence of a significantly non-diagonal sensing matrix.

The choice of a factor 10^{-3} for maximum tolerable power fluctuation is an educated guess that starts from the consideration than in Virgo+ we could reach 1% of stability of the carrier field. Since Advanced Virgo is aiming to have ten times better sensitivity, the goal for angular stability was also tightened by the same factor. More solid estimates might be computed once a proper simulation tool to compute the effect on sensitivity of a mirror mis-alignment will be available.

The requirements are driven by the carrier field fluctuations. Choosing the same requirements for the sidebands might at first seem in contrast with the assumption of 2% fluctuations made in sec. 1.3.5. However it is known from Virgo and Virgo+ commissioning experience that sideband fluctuations are very sensitive to any interferometer defects, mainly aberrations in the PRC. Since it is not possible as of today to properly estimate such effects, it was considered safe to compute the angular requirement on a tight basis, and assume a Virgo-like fluctuation to compute OMC requirements.

Port	Angular control	Beam centering
B1p	f1, **f2**, **DC**	2×f2
B2	f1, f2, **f3**	DC
B4	**f1**, **f2**	DC
B7	**DC**	
B8	**DC**	

Table 1.10: Quadrant diode demodulation frequency specifications. In bold signals used for the control

1.7.4 Quadrants and demodulations

The Automatic Alignment sensing scheme is based on a set of quadrant diodes placed at the detection ports shown in Figure 1.1. Each port is instrumented with two quadrants photo-diodes, one in near field (XX_A) and one in far field (XX_B). The use of two quadrants is important to be able to digitally combine the outputs to fine tune the Gouy phase of the error signal used for the angular control. To be able to obtain arbitrary phase in this way it is necessary that the two quadrants are placed in positions with 90 degrees of Gouy phase difference, which is a slightly less stringent requirement with respect to the near and far field placement. Even the Gouy phase difference between the two sensors does not need to be very accurate. A tolerance of ±20 degrees is assumed to be enough.

The power impinging on each quadrant diode is 25 mW, considering to have a maximum acceptable impinging power of 50 mW except for the B1p quadrant diodes which receive 2.5 mW of impinging power. These values are not finalized yet, but since for Virgo+ the high power quadrant diodes can accept 30 mW of impinging power, a maximum tolerance of 50 mW could be feasible. On the other hand the maximum allowed beam power for the B1p quadrants is 2.5 mW to be more conservative, since it is not clear up to now which is the amount of power at the dark port which can be extracted from the main beam for angular control. Clearly if the amount of power will be higher the signal to noise ratio will improve with a square root law.

All quadrants will be equipped with fast galvo centering system. The quadrants on the end benches will also need translation stages that might be used during the pre-alignment steps.

The quadrants have to be suspended in vacuum to reduce the spoiling of the signals, both demodulated and DC, due to seismic and acoustic noise. In Virgo and Virgo+, error signals, especially the DC ones, were dominated, below the Hz region, by air currents. Starting from 10 Hz, where there should be only shot noise, seismic motion was instead the limiting factor (see also sec. 1.7.7). It is important to mention that in Virgo and Virgo+ the error

signal used to control the Differential-End DOF, which is the most critical one in term of control noise, was dominated by the electronic noise given by analog to digital converters (ADC) non-linearities [29, 30, 31, 32]. The very large dynamical range needed for automatic alignment signals (typically of the order of 10^6-10^7) must be properly tackled in the design of the electronic read-out system.

For angular control, demodulated signals at all three main frequencies will be used. Needs for each port are summarized in tab. 1.10. Some signals will be used for angular control of the interferometer mirrors, some other to extract spot position to maintain the sensor well centered. Not all the signals coming from the detection ports are used in the present control scheme. These are highlighted in bold in tab. 1.10. Nevertheless in the commissioning phase the possibility to have a larger choice of signals, thus a flexible system, is mandatory. In Virgo the final control system has been developed in the years obtaining at the end a scheme which is completely different with respect to the one foreseen in simulations. This happened due to ITF imperfections and improvements and also due to the lack of complete and perfectly reliable alignment simulations.

Even for Advanced Virgo there is not a proper simulation tool available which allows to study the behavior of the alignment system as a function of possible unwanted effects (such as thermal effects, robustness versus interferometer working points etc...). As mentioned before the tools presently used are Finesse and Optickle. Optickle can take into account the radiation pressure effect, fundamental in the high power interferometers, but considers only the first higher order mode (not allowing the study of thermal effects, beam mismatches etc..) and no mirror static mis-alignments. On the other hand Finesse can take into account higher order modes but not radiation pressure effects. For all of these reasons, even if the control scheme which has been simulated and designed works properly in simulation, it is important to have enough flexibility and safety margins to be able to use a different control scheme with respect to the designed one, to deal with commissioning uncertainties and effects than could not be simulated nor foreseen.

1.7.5 Automatic Alignment control scheme

Sensing scheme

The Automatic Alignment control scheme has been modeled with Optickle, its control noise and the control accuracy for each angular degree of freedom have been evaluated with *Pickle* [33], the Optickle tool to propagate the angular control noise to the sensitivity, together with the residual mirror displacements, that was developed by the Advanced LIGO ISC group.

The only noise taken into account in the simulations is the shot-noise, thus if the sensing will be dominated by other sources of noise the angular control scheme has to be completely re-designed and the control noise re-evaluated. In other words all quadrant photo-diode signals are assumed to be shot-noise limited everywhere above 10 Hz.

In order to design the control scheme the sensing has been simulated by optimizing the amplitude of the transfer functions between the angular degree of freedom and the quadrant diodes tuning the Gouy and demodulation phases of the quadrants. The goal was to obtain the best decoupling of the angular degrees of freedom, taking care not to spoil the signal to noise ratio. In other words, whenever possible, the signal with larger SNR has been chosen.

It has been chosen to use a similar control scheme for all the three optical configurations (low, high power with and without SRC) in the sense that for each configuration a given angular d.o.f. is detected by the same detection port. Nevertheless, in each optical configuration parameters are re-tuned, such as demodulation and Gouy phases and control gains. Control filters are clearly different in the high and low power regime to take into account radiation pressure effects on the mechanical transfer function.

The optimal sensing scheme is the following:

- B1p demodulated at f_2 used for Differential(+)
- difference of the DC signals coming from the terminal benches for Differential(−)
- B2 demodulated at f_3 used for Common(+)
- sum of the DC signals coming from the terminal benches for Common(−)
- B4 demodulated at f_1 for PR
- B1p DC signal for SR (controlled in *Drift control mode*)
- B4 demodulated at f_2 for BS

Arm degrees of freedom control

The plane of the interferometer is kept fixed by the input beam control (not taken into account in these simulations) and the (-)-modes, controlled with a DC signals using B7 and B8 quadrants. At low frequency (about 3 mHz) the (-)-modes error signal will be substituted with mirror to beam relative centering signals to minimize the angular to longitudinal coupling. Such signals can be obtained using a dithering technique as done for the Virgo

input mirrors centering [29]. Otherwise, as recently proposed, processed camera images [34] might provide the needed signals.

A clear difference between the Virgo and the Advanced Virgo angular control is the suppression of the (+)-modes sensing due to the radiation pressure effects. Increasing the circulating power the (+)-modes become more and more stiff, reaching a mechanical resonance frequency of about 3.5 Hz at full power. The decoupling of the sensing matrix is also reduced, making the interferometer more sensitive to possible optical imperfections. As an example, the high power interferometer configuration becomes the most critical configuration for mis-tuning of the longitudinal working point, as it has been evaluated for the differential offset tuning [9].

Central cavity degrees of freedom control

The PR is controlled by using the first demodulation frequency while the BS using the second one. The BS and PR error signals can be exchanged if needed by retuning the Gouy and demodulation phases. It was chosen to use the best signal, in terms of SNR, for the PR since it is strongly coupled with the Differential(+), especially in the final configuration [9]. This sensing scheme should then assure the lowest PR control noise re-introduction in the Differential(+) mode.

The relaxed accuracy requirement for the SR (280 nrad) allows to adopt a hierarchical control strategy, using a low frequency control for the SR mirror with a band-width of some tens of mHz. This strongly simplifies the angular control decoupling. In Virgo the drift control developed for the input mirrors, which used a dithering technique to generate the error signals, achieved a control accuracy of about 100 nrad, which would be already compliant with the Advanced Virgo requirements for SR.

Discussion

After the control scheme was designed the sensor noise has been projected in the dark fringe. The requirement is, as in the longitudinal case, that all noise contributions must remain a factor 10 below the design sensitivity. In the angular control case this safety factor is even more important since it must also take into account the uncertainty in the simulation results.

In all the three studied configurations the control scheme is compliant with the specifications of control accuracy and control noise and it does not show any evident difficulties for the baseline design (as the decoupling of the sensing, the design of the control filtering etc...) [9]. The most critical degrees of freedom in term of control noise, for all the three configurations, are the

	PR	SR	BS
B4 f_1	103.4	0	-74.4
B1p A DC	0	1	0
B4 f_2	-2.1	0	-4.3

Table 1.11: Sensing for the central interferometer degrees of freedom in case of high power configuration with SR cavity, the most coupled configuration.

(-)-modes which are controlled with DC signals coming from the terminal benches. For this reason it is mandatory to have these sensors shot-noise limited. The performance of the end benches suspension becomes very important, see sec. 1.7.7.

In the power recycled only configuration at 25 W input power, the sensing is very well decoupled and the angular control noise is compliant with the factor 10 of safety below the sensitivity curve. Radiation pressure effects do not affect strongly the cavity modes. This configuration is the closest to the Virgo+ one. The experience gained in the past years will help the first commissioning phases.

In the dual recycled at 25 W configuration, the angular control scheme is very similar to the first one except for the introduction of the SRC. The Drift control applied to the SRC allows an easy decoupling of the signals which will help the implementation of an angular control compliant with the sensitivity requirements.

The final, dual recycled at full power configuration, which allows to reach the highest possible sensitivity, results to be compliant with the control noise sensitivity requirements. This configuration is the most critical one in terms of angular degrees of freedom decoupling, due to the (+)-mode sensing suppression and the presence of the SRC. The system is controllable, but its decoupling may become worrying as soon as optical defects occur in the real interferometer [9]. Indeed, in Virgo and Virgo+ we have experienced a strong coupling between the BS and PR mirror angular d.o.f. (a sensing ratio of 1:1) which made the commissioning and the implementation of the complete automatic alignment system longer and more difficult than initially foreseen. For instance up to VSR4, spring 2011, we could not control both degrees of freedom acting from the marionette. The PR had to be controlled by using the reference mass (which is noisier with respect the control from the marionette) due to the fact that in the PR error signal the BS resonances were visible and not mechanically damped. Table 1.11 shows the sensing matrix for the central interferometer degrees of freedom in the dual recycled configuration.

Moreover when some optical defects were present in the interferometer (such as thermal transients, higher order modes circulating in the cavities, not op-

timally tuned working point etc.) it was not possible to find two independent and noiseless signals to control both the BS and the PR mirrors. In VSR3 only the BS was globally aligned since the mis-tuning of the end mirror radii of curvature created lots of higher order modes which affected the angular error signal. The lack of a complete control system yielded a non-reliable working point affecting the detector duty cycle and sensitivity. These kind of issues will make the Advanced Virgo angular control system commissioning more complex and longer.

1.7.6 Performances of the angular control system

The performances of the designed control system can be quantified with the mirror residual motion in the AA closed loop configuration, and with the projection of angular control noise to the Advanced Virgo sensitivity. The control filters have been designed in order to meet the sensitivity requirements starting from 10 Hz, while the low frequency part of the controls has been tuned to meet, within a factor 2, the accuracy requirements. Further tunings are not useful at this step of the design, since the mechanical transfer function of the new payloads is not fixed yet. See figures 1.15, 1.16 and 1.17: bottom plots for control noise and top plots for accuracy performances.

The residual angular displacements and the AA control noise, evaluated with the Optickle simulation, are in agreement with the accuracy and the sensitivity requirements, for all the three configurations. The most critical degrees of freedom in terms of control noise are the (-)-modes, for all the three commissioning configurations.

In the final configuration, the high power dual recycled interferometer, the radiation pressure suppresses the (+)-mode sensing. The consequence is a worse mode reconstruction, especially for the Differential(+), which yield an excess of control noise. This fact is visible in Figure 1.17 where the control noise due to the Differential(+) mode, dashed blue line, is larger with respect to the B1p diode shot-noise contribution, blue line.

This behavior is not critical in simulation since the Differential(+) noise is far from the sensitivity, but the coupling can be stronger in a real interferometer leading to further increase of control noise.

1.7.7 Quadrant suspension requirements

The requirements for the quadrant suspension, tilt and translation, have been evaluated analytically for the DC signals in transmission to the long arm cavities used for the control of the (-)-modes [35]. As highlighted before these are the most critical degrees of freedom in terms of control noise.

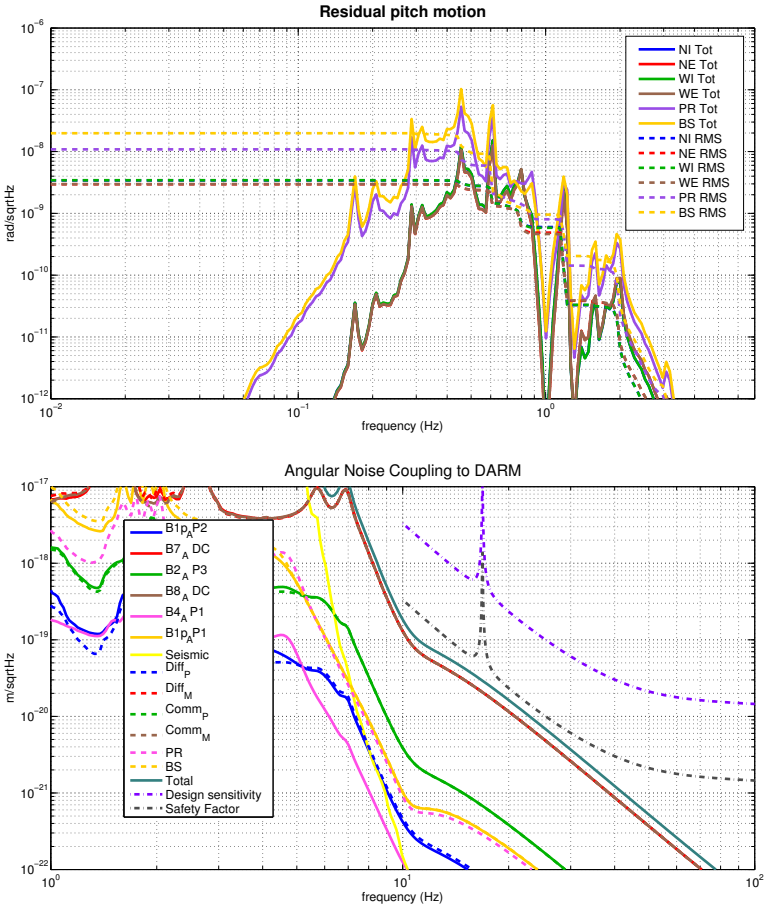

Figure 1.15: Mirror residual displacement and Automatic Alignment control noise projection for the first commissioning phase (low power interferometer without SRC) on the top and on the bottom plot respectively. The mirror residual motions are close to the accuracy requirements and improvement margins have been left in the filter design.

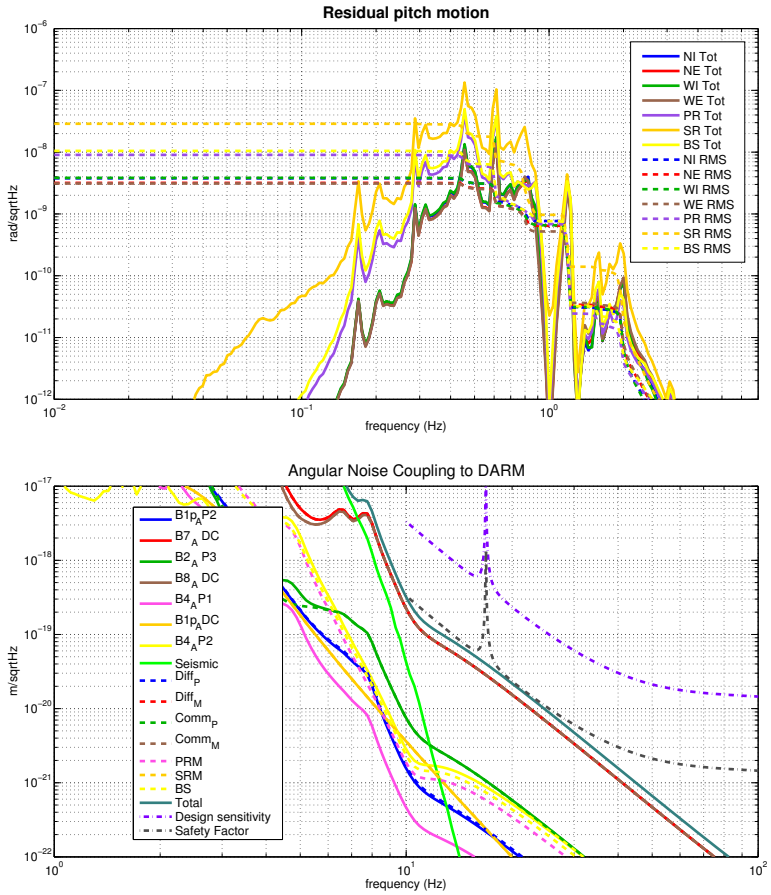

Figure 1.16: Mirror residual displacement and Automatic Alignment control noise projection for the low power interferometer with SRC on the top and on the bottom plot respectively.

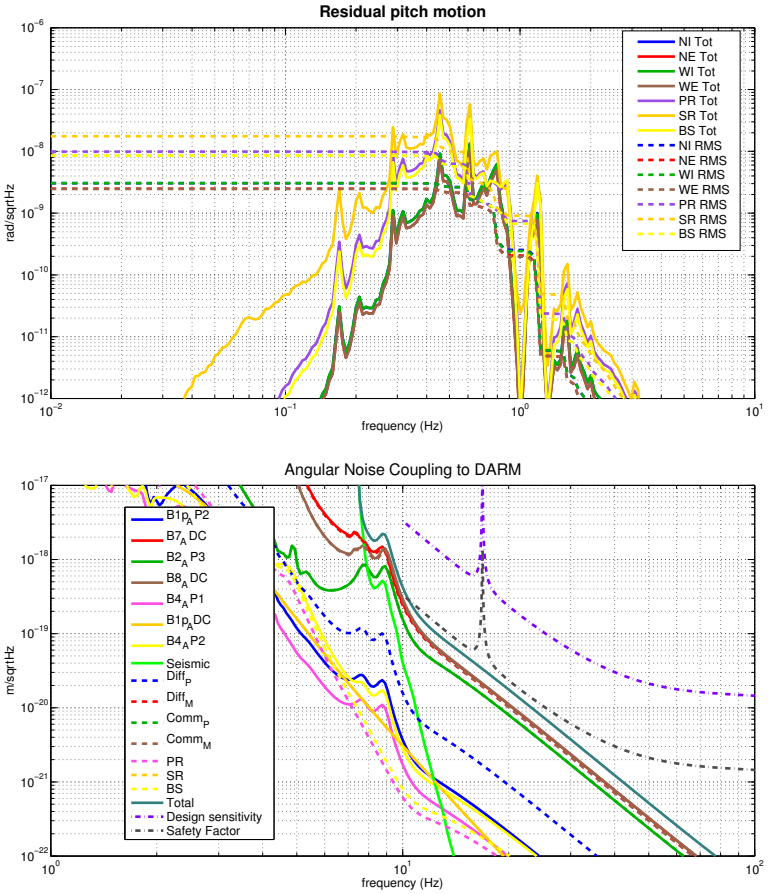

Figure 1.17: Mirror residual displacement and Automatic Alignment control noise projection for the final commissioning phase (high power interferometer with SRC) on the top and on the bottom plot respectively.

	Requirement	
δh	$2.4 \cdot 10^{-12}$	$m/\sqrt{Hz}$
$\delta\theta$	$3.4 \cdot 10^{-15}$	$rad/\sqrt{Hz}$
h_{RMS}	20 μm	
θ_{RMS}	0.027 μrad	

Table 1.12: Suspended terminal detection bench displacement requirements. Spectral requirements are valid above 10 Hz.

A DC signal measures the relative beam-quadrant displacement, thus any bench motion fakes the alignment signal generated by the beam displacement due to cavity mirrors misalignment. The bench motion has then to be low enough to not spoil the mode angular sensing at low frequency, inside the Automatic Alignment control bandwidth, i.e. up to few Hz. It must also not spoil the quadrant sensing noise at high frequency, in the detection bandwidth, i.e. above 10 Hz.

The requirements have been obtained at low frequency by analytically computing the amplitude of the angular error signal for the (-)-mode misalignment equivalent to the accuracy requirements (110 nrad see tab. 1.9) taking into account the quadrant diode dimension, the beam size at the quadrant and the telescope transfer function (bench translation and bench tilt to beam displacement on the quadrant) as given by the DET sub-system (baseline telescope design).

At low frequency the spurious signal coming from bench motion is required to be a factor 5 below the real angular error signal. For the high frequency requirements the maximum allowable bench displacement is set to have the equivalent signal below the shot noise of a factor 10. The results are listed in tab. 1.12.

The most critical requirement is for the residual tilt displacement (θ_{RMS}). The required accuracy is about a factor 3 below the Virgo+ test mass local control performances. Since the requirement in the translation direction is very loose, the telescope can be re-tuned to reduce the tilt-translation coupling of about a factor 3 to meet the typical local control performances, which are assumed to be possible also for suspended benches.

Moreover an additional low frequency control to point the beam on the terminal mirrors, by using the camera images to measure the relative position beam-mirror [34] has been recently proposed. It could relax the requirements only if it can be used with a control bandwidth larger than 500 mHz (to go above the micro-seismic region where the largest part of the bench motion is located). The limiting factor is the camera sensing noise which must be low enough to not reintroduce control noise in the automatic align-

ment error signal. Studies and noise evaluations are in progress, but for the moment this solution is not considered in the baseline design.

1.8 Software requirements

1.8.1 Fast real-time control

The real-time system that is currently used for both the lock acquisition and the steady state control consists of a chain of several components (ADC,Photo-diode read-out (Pr), Gc, Digital Signal Processor (DSP) and finally the Digital to analog converter (DAC)) that run at a sample frequency of 10 kHz. It is expected that the real-time software that will be used for the longitudinal control of Advanced Virgo will not be fundamentally different from the current one. Some minor work might be required to remove some legacy parts or update to the future software environment. The *locking algorithm* (which is part of Gc will probably be rewritten from scratch, which will be done in parallel with the commissioning activity.

The overall delay of all the components in the chain poses a limit on the unity-gain-frequency of the locking loops. As discussed in 1.3.6, there might be a need to increase the unity-gain-frequency to 400 Hz in case of a double-recycled interferometer, which is hard to achieve with the current system. A reduction of the delays will be necessary, for example by increasing the sample frequency or optimizing the anti-aliasing filters. This is discussed in more detail in [xx ref DAQ chapter].

The software chain used for controlling the angular degrees of freedom is pretty similar to the one used for the longitudinal part. The main difference is that it uses quadrant-detectors instead of photo-diodes and that the control process runs at a much lower frequency (2 kHz typically). Since this is about an order of magnitude slower than the control system used for the longitudinal controls, it poses no extra requirements on the digital or analog delays of the control system.

1.8.2 Slow control

Most of the slow control of Virgo is performed using Automation of the Locking Procedure (ALP) servers. The whole lock acquisition currently takes between 10 and 20 minutes. This process is driven by the AlpMain server, which basically executes a long lists of Cm commands that are sent to other processes, with the occasional waits and checks to see if a certain state is achieved. The whole sequence of the lock acquisition itself will have to be written from scratch, based on the experience of the commissioning.

In addition to this simple sequencing, a number of servos is active that implement slow feedback-loops for stabilizing e.g. a unity-gain-frequency of a certain loop. Also these are implemented in ALP (e.g. AlpLock, AlpTCS, etc.).

Since all the time-critical actions are performed using real-time systems and since ALP is mainly used to slowly change the configuration of the interferometer, the requirements on it are not very high. It should therefore be no problem to use ALP as it is now to implement the slow control of Advanced Virgo. ALP has, however, some limitations when it is used to implement complex logic (e.g. sub-functions, exceptions, inter-process communication) and advanced calculations (e.g. vector math as in Matlab). These kind of operations were already important in Virgo+ and are more critical in Advanced Virgo, given the increased complexity of the system. We therefore propose to investigate the possibility of using an existing scripting language in addition to or in place of ALP, instead of upgrading ALP to obtain such new features. The migration to the new architecture will be needed only at the time of restart of the commissioning activities, therefore this is not a priority task.

1.9 Interfaces with other sub-systems

The design of both longitudinal and angular control systems creates several interfaces with other subsystems. All the requirements are discussed in more details in the corresponding sections.

1.9.1 OSD

In order to control the power and signal recycling cavity longitudinal degrees of freedom a pick-off of the beam inside the recycling cavity is needed. This requires the addition of a plate in front of the power recycling mirror to extract such a beam.

1.9.2 MIR

The use of Etalon effect in the input mirrors to tune the interferometer finesse asymmetry is an important risk reduction strategy (sec. 1.3.10 and 1.3.9). This implies the need of having input mirrors with parallel faces. To meet the sensitivity requirements, in the power recycled case losses asymmetries must remain below 20 ppm and finesse asymmetry below 1% to be able to meet the requirements.

Frequency	**Phase noise [rad/$\sqrt{\text{Hz}}$]**	**Rel. ampl. noise [1/$\sqrt{\text{Hz}}$]**
6.3 MHz	$1.8 \cdot 10^{-6}$	$1.7 \cdot 10^{-7}$
56.4 MHz	$1.1 \cdot 10^{-6}$	$1.1 \cdot 10^{-6}$
8.4 MHz	0.27	$1.7 \cdot 10^{-7}$

Table 1.13: Summary of requirements for sideband amplitude and phase noise. Modulation noises enters in the photo-diode output signal following two paths. The first one is through the noise at the level of the modulation, which is transmitted to the laser beam and enters on one of the inputs of the mixer. The second path is through noise introduced by the local oscillator distribution system, which enters on the other input of the mixer. The requirements given here apply to the total of the two contributions.

The reflectivity of the power recycling pick-off plate is required to be about 300 ppm, in order to have enough power in the pick-off beam even with low input power (sec. 1.3.2).

Auxiliary lasers at a wave-length different from the main one (sec. 1.5) needs a careful evaluation of the mirror coating performances at the new wave-length. We ask to have an arm cavity finesse between 5 and 10 at 1319 nm for the coating of the mirror without changing the value of the 1064 nm parameters. This requirements have already been obtained for the mirror installed in the CALVA platform [4].

The angular control system foresees the use, even in science mode configuration, of signals coming from quadrants in transmission of the end mirrors. In order to have a suitable amount of power in the beam a lower limit for the end mirror transmission must be set. In the case of low input power (25 W), a transmission of 1 ppm gives about 150 mW of power on the end benches, which seems a reasonable amount to be shared between diodes, quadrants and cameras. Therefore the end mirror transmission should be $T \geq 1$ ppm.

1.9.3 INJ

The lock acquisition procedure might be strongly affected by radiation pressure issue. Moreover initial commissioning activities will be for sure carried out in a reduced input power regime. Both these considerations indicate the need of a system to continuously and smoothly tune the input power from its minimum values up to the maximum.

Requirements on modulation phase and amplitude noise have been computed, based on the steady state longitudinal control design. They are summarized in tab. 1.13 (see sec. 1.3.7 for more details).

	Requirement	
δh	$2.4 \cdot 10^{-12}$	$m/\sqrt{Hz}$
$\delta\theta$	$3.4 \cdot 10^{-15}$	$rad/\sqrt{Hz}$
h_{RMS}	20 μm	
θ_{RMS}	0.027 μrad	

Table 1.14: Suspended terminal detection bench displacement requirements.

1.9.4 SBE

The end mirror transmitted beams will be sensed by two quadrant photodiodes for each port. Spot position (DC) signals will be used to control two angular degrees of freedom. Their required accuracy gives limits on the spurious signal created by bench motion, which should give a contribution not larger than what would be equivalent to a beam translation inside the arm cavity of the order of 20 μm. Provided the magnification properties of the telescope (designed to reduce the beam size to a reasonable value which will fit the sensor) the spot motion on the quadrant can be converted to angular and translational residual motion of the end benches. The requirements obtained in this way are quite stringent and reported in tab. 1.14 (see sec. 1.7.7 for more details). Since the angular requirement is pretty tight, it was considered important to try an optimization of the telescope design to reduce the coupling from bench angular motion to spot displacement on the quadrant. This would relax the requirement on the bench angular motion. We can even afford some worsening on the coupling from bench translation to spot displacement on the quadrant, since the bench requirement with the present telescope is not very tight.

There are additional requirement on the bench motions inside the detector band-width, above 10 Hz. In order to have error signals dominated by shot noise, the maximum bench motion can be computed. With the present telescope design the required maximum bench motions are summarized in tab. 1.14 (see sec. 1.7.7 for more details).

1.9.5 DET

The different demodulation frequencies needed at each port are summarized in tab. 1.15. In all ports the two quadrants should be placed in such a way to have the Gouy phase difference between them as close as possible to 90 degrees. In this way the signals from both quadrants could be mixed digitally to reconstruct with high accuracy the needed Gouy phase. This is necessary to proper decouple the angular degrees of freedom (sec. 1.7.4). All quadrants will use galvo fast centering systems.

Port	**Photo-diodes**	**Quadrant photo-diodes**
Symmetric port (B2)	DC, f_1, $3f_1$, f_2, f_3	DC, f_1, f_2, f_3
Dark port after OMC (B1)	DC	
Dark port before OMC (B1p)	DC, f_1, f_2, $2f_1$, $2f_2$	DC, f_1, f_2, $2f_2$
OMC reflection (B1s)	DC, f_1, f_2, $2f_1$, $2f_2$	
Power Recycling pick off (B4)	DC, f_1, f_2, $2f_1$, $2f_2$	DC, f_1, f_2
Arm cavity transmission (B7, B8)	DC , f_1	DC

Table 1.15: Needed signals and demodulation frequencies at each interferometer output port.

Frequency [MHz]	PR 25 W	SR 25 W	SR 125 W
6	1/120	1/7	1/36
56	1/1700	1/460	1/2300

Table 1.16: Filtering requirements (in power) for the OMC in different interferometer configurations.

The requirement on the DARM longitudinal control loop (sec. 1.3.4), which comes from ISC considerations, have an impact on design requirements of the OMC. Any fluctuation of spurious fields (sidebands or higher order modes) transmitted by the OMC is directly translated to a motion of the DARM degree of freedom, thus spoiling the loop accuracy (sec. 1.3.5). From these considerations a requirement on the maximum sideband power which can be tolerated in transmission of the OMC is obtained to be of the order of 0.07 mW. This poses stringent limits on the OMC filtering capabilities. Tab. 1.16 summarizes the filtering requirement in different configurations, using the estimate of sideband powers at the input of the OMC given in [36].

As anticipated in the INJ interface description, requirements on modulation phase and amplitude noise have been computed, based on the steady state longitudinal control design. These requirements are given in term of the total phase and amplitude noises at all mixer inputs, and therefore apply also to the local oscillator distribution network. A summary can be found in sec. 1.3.7 and tab. 1.13.

As explained in the previous subsection concerning the interface with SBE, angular accuracy requirements might request an optimization of the end benches telescope in order to reduce the coupling of bench angular motion to spot displacement on the quadrant. A summary can be found in sec. 1.7.7 and tab. 1.14.

Most of the photo-diode and quadrant signals will have very large dynamical range (typically 10^6-10^7 in Virgo+ angular signals). The full read-out chain must be able to handle such large dynamics, without introducing up-

Configuration	10 Hz	100 Hz	1000 Hz
PR 25 W	$2 \cdot 10^{-8}$ Hz$^{-1/2}$	$1.5 \cdot 10^{-8}$ Hz$^{-1/2}$	$2 \cdot 10^{-8}$ Hz$^{-1/2}$
SR 125 W	$4 \cdot 10^{-9}$ Hz$^{-1/2}$	$9 \cdot 10^{-9}$ Hz$^{-1/2}$	$9 \cdot 10^{-9}$ Hz$^{-1/2}$

Table 1.17: Summary of RIN requirements at the interferometer input. For the full dependence on the frequency refer to fig. 1.4 and 1.7.

conversion noise.

Auxiliary lasers (sec. 1.5) will go through the detection benches. Proper space to allow the needed optical path must be prepared. Since a different wavelength will be used we will need a special dichroic element to separate the beams and also avoid any perturbation on the signals observed with the 1064 nm laser. For the latter point some beam dumpers may also be needed.

Time-domain simulations done at LIGO suggest that in case of an unlock of a double-recycled interferometer, a large part of the optical power stored in the interferometer (around 50 Joule) will exit the asymmetrical port in a very short time (less than 20 ms). Since the damage-threshold of a typical photo-diode is on the order of 100 mJ, a very fast shutter is needed. To not cause any damage, the shutter must be almost completely closed within 1-2 ms after receiving a trigger, which might be based on the DC-power crossing a certain threshold [7]. This seems pretty demanding for a standard mechanical shutter.

DET sub-system fixed the DC-read-out offset value in order to have a carrier power at dark port of 80 mW. From the point of view of ISC, it would be better to reduce as much as possible the offset. As explained in [9] the larger the offset the more coupled the angular sensing matrix becomes.

1.9.6 PSL

The lock acquisition of the long arms requires the residual frequency noise with pre-stabilized laser to be significantly smaller than the cavity linewidth, namely smaller than about 1 Hz RMS.

Considering the coupling of frequency and power noise at the interferometer input to the detector sensitivity in presence of some reasonable asymmetries, it is possible to draw requirements for the stabilization loops. This is in particular important for the power stabilization at the IMC transmission. The required relative intensity noise (RIN) depends on the interferometer configuration (sec. 1.3.8). A summary of the requirements are given in tab. 1.17. More details are given in fig. 1.4 and 1.7.

1.9.7 DAQ

All the control loop designs have been carried out without considering the effect of delays introduced by the real-time control system. Such delays might play an important role only in the case of the DARM loop for dual recycled configuration, which has a unity gain frequency of about 400 Hz [6]. This would impose a requirement on the total delay of about 50 μs which according to the DAQ subsystem would be difficult to reach. Therefore it is necessary to re-consider the design of the control. It seems feasible, although not yet designed, to reduce the band-width to 200 Hz. This would relax the delay requirement to about 100 μs.

The automation of the entire lock procedure and the steady state operations requires an infrastructure to implement scripting and slow servo loop, as was done in Virgo using ALP. A greater flexibility with respect to the scripting and computational capabilities of ALP would be very useful (sec. 1.8) to improve the lock acquisition robustness and speed up the commissioning.

1.9.8 SAT

The issue of total delay in the DARM loop involves also the SAT subsystem, since part of the delay must be accounted to the DSP, coil drivers and DAC controlling the mirror actuators.

The performances of the inertial damping system are important for the total residual RMS motion of the mirrors. Indeed the RMS is almost completely accumulated at frequencies below 1-2 Hz. The requirements for the longitudinal control accuracy are met by the control loops, assuming the payload motion is the same as measured in Virgo (about 0.5 μm and 0.1 μrad RMS). This implies that the mirror motion in Advanced Virgo must not be larger than the Virgo one. Moreover, any reduction of the mirror low frequency motion at the level of the suspension system will help implementing more stable and less noisy longitudinal control loops.

1.9.9 PAY

The force needed to acquire and maintain the interferometer lock can be estimated starting from simple modeling and experimental verifications. The use of non-linear lock acquisition, which was experimentally proved in Virgo+, reduces the maximum force needed in high power of about a factor 160 with respect to the Virgo+ actuators (sec. 1.4.1). A rough estimation indicates that the maximum force used in Virgo+ was of the order of 3 mN per coil-pair. Keeping some safety margin, we can expect to reduce this by

a factor 5-10. The exact value is still to be decided and depends on the mechanics of the new payload and on the amount of sensor noise during the lock acquisition.

Early re-allocation to the marionette also virtually eliminates any requirement on the maximum actuation force on the mirror, from the need to maintain the lock.

The need of increasing the DARM loop band-width poses stringent requirements on the minimum possible frequency of internal resonances of the structure holding the actuation coils. The present design of the DARM control foresee and band-width of 400 Hz. Having all resonance above this frequency seems very difficult, therefore it is necessary to re-consider the design of the control. It seems feasible, although not yet designed, to reduce the band-width to 200 Hz.

1.9.10 INF

In the terminal stations, the space for auxiliary laser benches must be allocated near the mini-tower and on the same concrete slab. We need to check with the infrastructure group the safety issues, as we will be placed on the roof of the clean room. We may also need an acoustic enclosure and we may be able to reuse the one installed around the end arm optical tables.

1.10 Summary and conclusions

The conceptual design of the steady state control of Advanced Virgo, both for angular and longitudinal degrees of freedom, is concluded. Three different configurations have been studied: power recycled only at low input power, dual recycled at both low and full input power.

To be compliant with the detector scientific goal all control noises must remain a factor 10 below the design sensitivity in all studied configurations. To reach such performances the sensing noise of all the error signals cannot exceed the shot noise level, given the maximum power that can be sensed, as set by the DET subsystem.

The accuracy requirements for the control system have been computed based on considerations on the maximum tolerable power fluctuations and on noise up-conversion. The control systems are compliant with such accuracy constraint, provided that some requirements to other subsystems are fulfilled. In particular the longitudinal control poses constraints on the OMC performances and the angular ones on the end benches seismic attenuation system. Requirements on the laser technical noises at the interferometer input and

on the interferometer asymmetries are also derived. The need of a precise matching of the two input mirror reflectivities dictates the need of the Etalon effect and its control.

The performances of the ISC control system have been evaluated using modal simulation tools, namely Finesse and Optickle. The uncertainty in the modeling and in the simulation results is still large. Indeed the large circulating power leads to strong radiation pressure effects. Such effects can be modeled only using Optickle, which on the other hand cannot use higher order modes and therefore does not give completely accurate results in particular for the angular controls. A tool capable of simultaneously handle higher order modes and radiation pressure would be very important. Plans for the development of such a tool are being considered, compatibly with the available manpower.

The study of the lock acquisition procedure has started only since few months. The lock acquisition of a single arm, even with the increased finesse of Advanced Virgo, will not pose fundamental difficulties. It was shown in simulation and experimentally in Virgo+ that low force lock acquisition techniques are available, allowing a reduction of the needed maximum actuation force at the level of the mirrors.

In the case of power recycled only interferometer, which will be the first one to be commissioned, the same locking algorithm implemented in Virgo and Virgo+ will be used. The optical configuration is very similar and there are no differences that will make the Variable Finesse technique inadequate. We expect to acquire the lock at reduced power and then increase it to the running one when the interferometer is in a well controlled state. If we use a MICH offset, the switch to DC readout will pose no fundamental difficulty since the controlled system will remain open-loop stable.

The lock acquisition procedure in the dual recycled case has not been studied in depth so far. We expect to be able to profit from the use of auxiliary laser to maintain the arm cavity locked while acquiring the control of the central part of the interferometer. This would imply a completely different locking scheme with respect to the power recycled case. Another possible strategy that will be considered in the next months is an extension of the Variable Finesse technique.

A risk reduction strategy to cope with sideband aberrations due to thermal effects and mirror defects is proposed. It foresees the use, during the thermal compensation system commissioning, of an additional high frequency modulation. The corresponding sidebands will have very low recycling gain and therefore will be poorly sensitive to recycling cavity defects, providing reliable control signals.

Bibliography

[1] A. Freise, at al. , *Frequency domain interferometer simulation with higher-order spatial modes*, Class. Quant. Grav. 21 (2004) S1067 [arXiv:gr-qc/0309012] 2, 35

[2] Optickle home-page, `http://ilog.ligo-wa.caltech.edu:7285/advligo/ISC_Modeling_Software` 2, 4, 35

[3] H. Yamamoto et al., *End to End* time-domain optical simulator `http://www.ligo.caltech.edu/~e2e/` 2, 29

[4] CALVA home-page, `http://calva.lal.in2p3.fr/` 50

[5] R. Gouaty, *Requirements for longitudinal and quadrant photo-diodes*, VIR-0438A-11 (2011) 2, 8

[6] G. Vajente, *Advanced Virgo Length Sensing and Control steady state design*, VIR-0738A-11 (2011) 5, 8, 9, 12, 14, 54

[7] L. Barsotti and M. Evans, *Lock Acquisition Study for Advanced LIGO*, LIGO technical note LIGO-T1000294-v1 (2011) 30, 53

[8] G. Vajente, R. Day, J. Marque, *AdV optical layout: new parameters proposal*, VIR-0377B-11 (2011) 5, 34

[9] M. Mantovani, *Differential offset vs Automatic Alignment control*, VIR-0737A-11 9, 41, 42, 53

[10] E. Tournefier, *Advanced Virgo output mode cleaner: specifications*, VIR-0071A-08 (2008) 11

[11] J. Marque, G. Vajente, *Proposal of an alternative design of the OMC to improve filtering performance*, VIR-0713A-11 (2011) 11

[12] B. Swinkels, E. Campagna, G. Vajente, L. Barsotti and M. Evans, *Longitudinal noise subtraction: the alpha-, beta- and gamma-technique*, VIR-0050A-08 (2008) 13

[13] E. Tournefier, *High frequency noise in the recycled ITF*, VIR-0154A-05 (2005) 16

[14] A. Chiummo, *Coupling of frequency and power noise vs. ITF asymmetries: preliminary results*, VIR-0485A-11 (2011) 17

[15] A. Chiummo, *Requirements for technical noise with ITF asymmetries*, VIR-0517A-11 17, 22

[16] R. Gouaty, *OMC design & specifications for side band transmission*, VIR-0581A-11 22

[17] F. Bondu, *L'interferometre Virgo: proprietes optiques, stabilisation en frequence du laser*, Memoire d'habilitation a diriger des recherches, Observatoire de la Cote d'Azur (2008) 23, 33

[18] E. Calloni, G. Vajente, *Conceptual design of the second stage of frequency stabilization for Advanced Virgo* VIR-0013A-12 7, 23, 28

[19] B. Swinkels, P. Ruggi and G. Vajente, *Lock acquisition of the Advanced Virgo arm-cavities with reduced force*, VIR-0019A-12 (2012) 25

[20] F. Acernese et al., *Lock acquisition of the Virgo gravitational wave detector*, Astroparticle Physics vol. 30 p. 29, (2008) 25

[21] F. Cavalier, *Lock acquisition for the arms*, VIR-0656A-10 31

[22] B. Canuel et al, *AdV INJ: Preliminary Design Study document*, VIR-0023A-09 32

[23] D. Sigg *et al.*, *Phys. Lett. A* **354** 3 (2006) 167-172 . 35

[24] M. Mantovani, *Automatic Alignment control scheme & Terminal bench requirements update*, VIR-0444A-11 36

[25] M. Mantovani, *Automatic Alignment Sensing and Control scheme for Advanced Virgo MSRC configuration*, VIR-0201A-11 37

[26] M. Mantovani, G. Vajente, *Alignment accuracy requirements for Advanced Virgo*, VIR-0247A-10 37

[27] M. Mantovani, *Stable Recycling Cavities : L.R.C. vs S.R.C. angular requirements*, VIR-0029B-11 37

[28] M. Mantovani for the Virgo Collaboration, *Automatic Automatic Alignment for the first science run of the Virgo interferometer*, Astroparticle Physics Volume 33, Issue 3, April 2010, Pages 131-139 37

[29] M. Mantovani for the LIGO-Virgo Collaboration, *Automatic Alignment system during the second science run of the Virgo interferometer*, Astroparticle Physics Volume 34 (2011) 327-332 37, 39, 41

[30] M. Mantovani, *Automatic Alignment status for VSR2 and plans toward V+ sensitivity*, VIR-0513A-09 (2009) 39

[31] M. Mantovani, *AA electronics status and future installations*, VIR-0208A-10 (2010) 39

[32] M. Mantovani, A. Masserot, Virgo logbook entry 24766 (2009); M. Mantovani, Virgo logbook entry 25217 (2009); M. Mantovani, A. Masserot, F. Paoletti, Virgo logbook entry 26695 (2010) 39

[33] L. Barsotti, M. Evans, *Modeling of Alignment Sensing and Control for Advanced LIGO*, LIGO-T0900511-v4 39

[34] B. Mours, *Beams centering using cameras*, VIR-0654A-11 41, 47

[35] M. Mantovani, *SEB displacement requirements update*, VIR-0523A-11 43

[36] R. Gouaty, *OMC design & specifications for side band transmission*, VIR-0581A-11 (2011) 52

[37] R. Abbott, R. Adhikari, S. Ballmer, L. Barsotti, M. Evans, P. Fritschel, V. Frolov, G. Mueller, B. Slagmolen, S. Waldman, *AdvLIGO Interferometer Sensing and Control Conceptual Design*, LIGO-T070247-00-I (2008) 2

[38] H. Grote, *High power, low-noise, and multiply resonant photodetector for interferometric gravitational wave detectors*, Rev. Sc. Instr. 78, 054704 (2007) 2

[39] E. Tournefier, *Technical noises for Virgo+: DC and AC readout cases*, VIR-NOT-LAP-1390-338 3

[40] The Virgo Collaboration, *Advanced Virgo Baseline Design*, VIR-027A-09 3